NASA CONTRACTOR
    REPORT

NASA CR-173666

WAKES FROM ARRAYS OF BUILDINGS

By Earl Logan, Jr. and Shu-Ho Lin
College of Engineering and Applied Sciences
Arizona State University
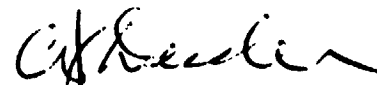Tempe, Arizona 85287

Final Report, Contract NAS8-34318

November 1982

Prepared for

NASA-George C. Marshall Space Flight Center
Marshall Space Flight Center, Alabama 35812

1. REPORT NO. NASA CR-170666	2. GOVERNMENT ACCESSION NO.	3. RECIPIENT'S CATALOG NO.
4. TITLE AND SUBTITLE Wakes from Arrays of Buildings		5. REPORT DATE November 1982
		6. PERFORMING ORGANIZATION CODE
7. AUTHOR(S) Earl Logan, Jr. and Shu-Ho Lin		8. PERFORMING ORGANIZATION REPORT #
9. PERFORMING ORGANIZATION NAME AND ADDRESS College of Engineering and Applied Sciences Arizona State University Tempe, Arizona 85287		10. WORK UNIT NO.
		11. CONTRACT OR GRANT NO. NAS8-34318
		13. TYPE OF REPORT & PERIOD COVERED
12. SPONSORING AGENCY NAME AND ADDRESS National Aeronautics and Space Administration Washington, D.C. 20546		Contractor (Final Report)
		14. SPONSORING AGENCY CODE

15. SUPPLEMENTARY NOTES
Prepared for Atmospheric Sciences Division, Space Science Laboratory, Science and Engineering Directorate, George C. Marshall Space Flight Center, Alabama 35812
Technical Monitors: Dennis W. Camp and Margaret Alexander

16. ABSTRACT

Experiments have been carried out in a small wind tunnel in which atmospheric flow around buildings was simulated. Arrays of one, two, three, and four model buildings were tested, and wake profiles of velocity and turbulence were measured. The data indicate the effect of the buildings on the wind environment encountered by aircraft during landing or takeoff operations. It was possible to use the results to locate the boundaries of the air regions affected by the obstacles and to recommend preferred arrangements of buildings to maximize flight safety.

17. KEY WORDS Wind Tunnel Wind Shear Low-Level Flow Induced Flow	18. DISTRIBUTION STATEMENT Unclassified—Unlimited A. J. DESSLER Director, Space Science Laboratory

19. SECURITY CLASSIF. (of this report) Unclassified	20. SECURITY CLASSIF. (of this page) Unclassified	21. NO. OF PAGES 128	22. PRICE NTIS

MSFC - Form 3292 (May 1969)

FOREWORD

This study was initiated to determine wake profiles behind buildings and natural obstacles using a scaled model in a wind tunnel. The wind tunnel approach is preferable because of economy of time and money, simplicity and convenience. This is the fifth report of a program sponsored by the Fluid Dynamics Branch, Atmospheric Sciences Division of Space Science Laboratory at the George C. Marshall Space Flight Center, National Aeronautics and Space Administration, Huntsville, Alabama.

This research was conducted under the technical direction of Mr. Dennis W. Camp and Mrs. Margaret Alexander of the Space Science Laboratory at Marshall Space Flight Center. The support for this research was provided by Mr. A. Richard Tobiason of the Office of Aeronautics and Space Technology, NASA Headquarters, Washington, D.C.

ACKNOWLEDGMENTS

The authors were greatly assisted in the laboratory by Mr. Mike Canady, who produced the photographs of the surface flows; by Mr. Robert Field, who took the measurements with the 3-dimensional probe; and by Mr. Daniel Johnson, who assisted in taking the hot-film data.

TABLE OF CONTENTS

iv

LIST OF ILLUSTRATIONS (Continued)

LIST OF ILLUSTRATIONS (Continued)

LIST OF ILLUSTRATIONS (Continued)

LIST OF TABLES

NOMENCLATURE

Symbol	Definition
A	Slope of the velocity profile
$A_1, \ldots, A_5$	Control-surface areas
B	Constant
C_D	Drag coefficient
C_f	Friction coefficient
C_L	Lift coefficient
C_p	Pressure coefficient
D	Drag
H	Height of building
L	Length of buildings
l	Mixing length
S	Spacing between buildings
U	Longitudinal mean velocity
U_R	Reference velocity
U_1	Free stream mean velocity
U^*	Friction velocity
$\overline{uv}$	Component of Reynolds shear stress
u'	RMS value of longitudinal turbulence fluctuation
u'_m	Maximum value of u'
u'_0	RMS value of upstream turbulence fluctuation
V	Vertical mean velocity
W	Lateral mean velocity or width of building
x	Longitudinal coordinate
y	Distance from floor of wind tunnel
z	Lateral coordinate

GREEK ALPHABET

Symbol	Definition
δ	Boundary layer thickness
δ_i, δ_s	Upper and lower limits of high-velocity-gradient region
δ_m	Distance y at which $u' = u'_m$
ν	Kinematic viscosity
θ	Momentum thickness
τ_o	Surface shear stress

CHAPTER 1

INTRODUCTION

1. Applications of Wind Tunnel Research

Cermak (1975) has traced the beginnings of experimental studies of wind effects to the eighteenth century. In the last fifty years wind tunnel development has made possible many studies involving simulated wind passing around buildings and other structures. Such studies, coupled with the development of the principles of dimensional analysis, have made possible the prediction of forces and moments created by atmospheric wind.

In recent years wind tunnels have been used to investigate the flow field around buildings to aid in th prediction of the spread of pollutants from factories and automobiles and to predict the wind environment of pedestrians, land vehicles and aerospace vehicles in the immediate vicinity of buildings. Besides buildings, natural topography can affect the flow structure of the atmosphere, as can towers, fences and vegetation. The present work is concerned with the latter wind effect, viz., the effect of buildings or other obstacles on the wind environment of aerospace vehicles in flight.

2. Background of the Present Investigation.

Prediction of takeoff and landing trajectories of aerospace vehicles requires an advance knowledge of wind conditions in the field of operation. It is known that buildings in the vicinity of landing strips can affect the velocity profiles of the wind field. Wakes from

bluff bodies, as a potential hazard to air traffic, has been discussed by Fichtl, Camp and Frost (1977).

NASA Marshall Space Flight Center initiated work to relate building geometry to wake flow. Results of a field investigation was reported by Frost, et al (1977), and a wind tunnel investigation was described by Woo, Peterka and Cermak (1977). The data of the above field and wind-tunnel tests have been compared by Logan and Camp (1978). The effect of an upstream obstacle on the wake of a second (downstream) obstacle was investigated by Logan and Chang (1980). The interaction of wakes from laterally spaced buildings was reported by Logan and Barber (1980) and by Logan and Lin (1982).

The work cited above involved the effect of the spacing of very long (two-dimensional) buildings. In the present work buildings of finite length are considered. Building models are arranged in patterns of one, two, three or four buildings, and measurements of velocity and turbulence in the wake region are obtained. The results show the effect of building length and spacing on the wake character. The study pro-vides data which are useful for the prediction of the flight path of aerospace vehicles which are landing or taking off in the vicinity of single-or multiple-building arrays. The information is useful for the planning of new structures in the vicinity of airports.

3.   Single Buildings

Figure 1 was extracted from a report by Holdredge and Reed (1956). Using models of block-type buildings in a low-speed wind tunnel, the basic features of flow behind the buildings were studied through flow visualization. In the recirculation zone flow over the building is

2
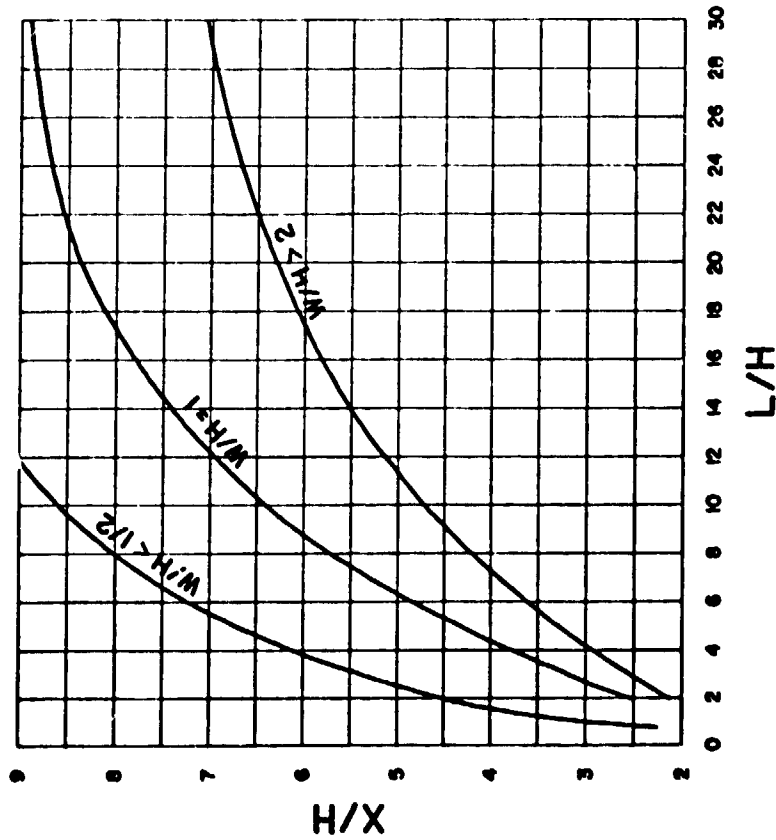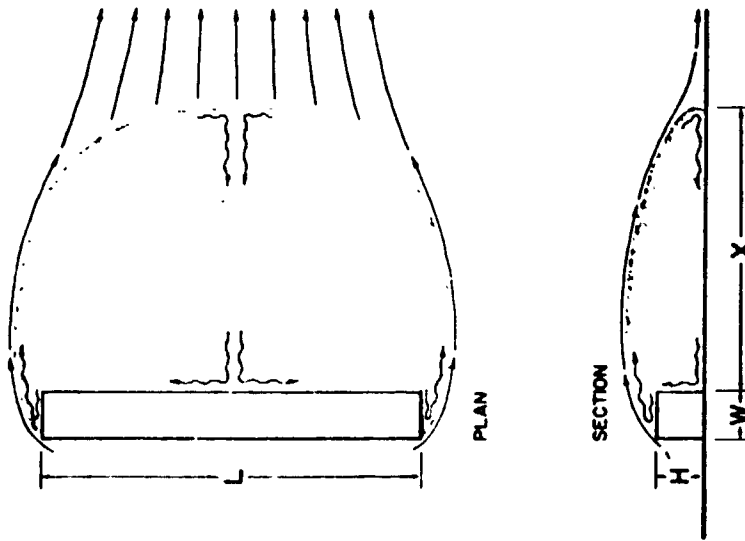
Fig. 1. Recirculation Zones from Smoke Tests of Holdredge and Reed
(1956)

accompanied by a reversed flow at ground level. Flow around the ends of the building is partly returned via an inward flow towards the back side of the building. These two secondary motions accompany the main flow around the single building and characterize the recirculation region.

The length of the recirculation zone for a two-dimensional model (large L/H) of square cross-section should be slightly less than nine, according to Fig. 1. This is in excellent agreement with the results of Logan and Barber (1980) obtained from skin friction values.

Figure 2 was also presented by Holdredge and Reed (1956) and illustrates surface pressure variation. Pressure taps were drilled through the walls of ⁿlexiglas models in a grid pattern. The results were then presented as contours of surface pressure coefficients on the five exposed faces of the block-type building. On the front face a region of high pressure $(C_p > .9)$ is indicated. The pressures are below atmospheric on the tor, side and back faces, as these faces are in contact with regions of separated flow. The cavities formed by the separated flow contain some fluid moving counter to the main flow direction. The pressure contours indicate probable flow direction along surfaces, e.g., on the back surface flow is expected to occur outward from the region interior to the $C_p = -.4$ contour, i.e., towards the end and the top surfaces, where $C_p < -.4$. The flow patterns are as indicated in Fig. 1, which are obtained by flow visualization.

The present investigation extends the work of Holdredge and Reed (1956) to include wake profiles of velocity and turbulence. The present work also involves surface flow patterns on the ground in the cavity behind the model.

4
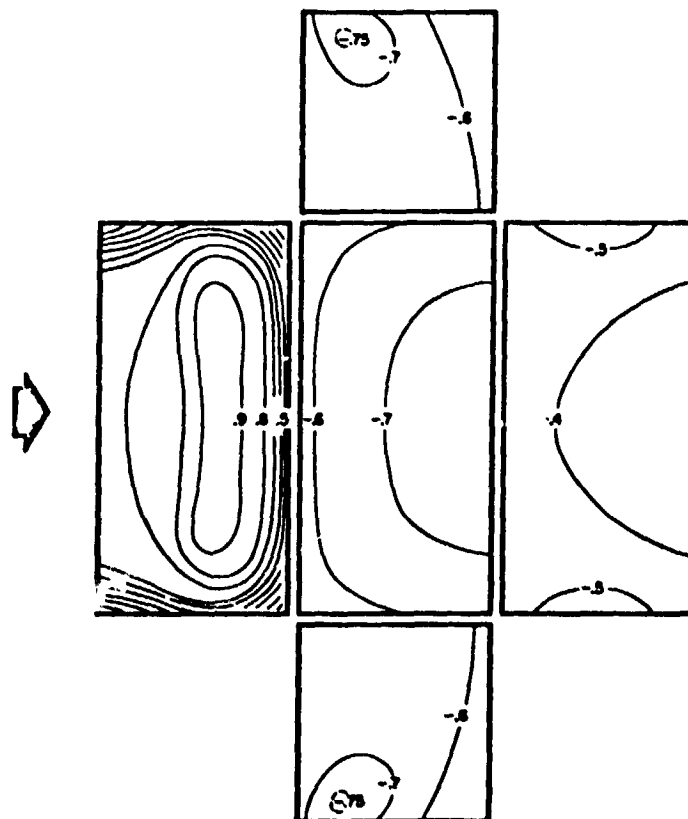
l:l:2

Fig. 2. Pressure Coefficients on the Surfaces of a Building [Holdredge
and Reed (1956)]

5

4.   Multiple Building Arrays

Holdredge and Reed (1956) also investigated the flow of air around arrays of buildings, including most of the patterns used for the present work. Their emphasis was different, in that only surface pressure measurements were reported. Their work shows the effect of building spacing on centerline surface pressures. The present work extends their investigation to include velocity and turbulence profiles downstream of building arrays and surface flow patterns obtained from flow visualization.

Penwarden and Wise (1975) obtained surface flow patterns, as well as velocity and surface pressure measurements for multiple building arrays. The thrust of this work, as well as the earlier work of Wise, Sexton and Lillywhite (1965), was to define the wind environment between buildings. The present work is geometrically similar but extends the work to include wake measurements downstream of the arrays.

5.   Theoretical Considerations

Some important theoretical ideas about flow around single buildings were advanced by Hunt (1971). He presents expressions which relate the force or moment on a building to the velocity field. Referring to Fig. 3 the drag coefficient on a block-type building is given by

$$C_D = \frac{1}{HLU_R^2} \left[\iint_{A_1} U^2 \, dy\, dz - \iint_{A_2} U^2 \, dy\, dz \right.$$

$$\left. - \iint_{A_3} UV \, dx\, dz - 2 \iint_{A_4} UW \, dx\, dy - \iint_{A_5} \tau_0 \, dx\, dz \right] \tag{1.1}$$

6
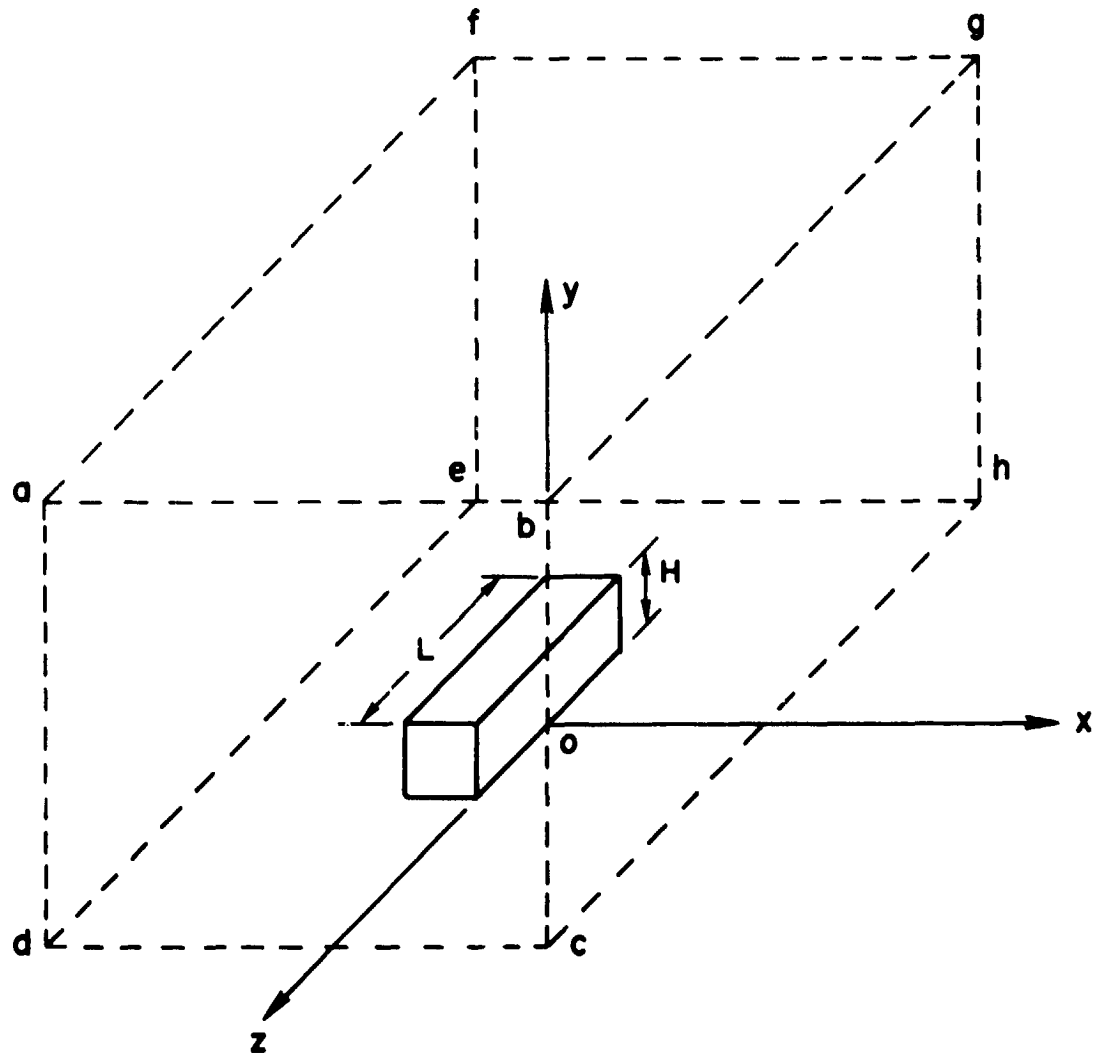
Fig. 3. Control Volume for Drag Calculation

where A_1 refers to area afedv, A_2 to area bghcb, A_3 to area afgba, A_4 to area abcda (or area efghe) and A_5 to area dehcd. These areas are the plane control surfaces of a box-like control volume surrounding the building, which is situated at the origin. The reference velocity U_R, used to non-dimensionalize the expression, is arbitrary and could be the freestream velocity U_1, the velocity U_H at $y = H$ in the upstream profile or an average velocity based on that part of the profile between $y = 0$ and $y = H$. The surface shear stress τ_0 and the velocity components U, V and W vary over the areas of integration.

Although the drag force D can be increased by increasing building length L, height H or the wind velocity U_R, the drag coefficient is modified when certain dimensionless ratios are altered. Joubert, Perry and Stevens (1971) indicate that this dependency might be given as

$$C_D = f (H/\delta, HU*/ , L/H) \tag{1.2}$$

where δ denotes boundary layer thickness, $U*$ upstream friction velocity and kinematic viscosity. Modification of the quantities on the right hand side of (1.2) changes the streamline pattern, and the surface pressure contours are likewise altered. Referring to Fig. 2, it is seen that a shorter building would yield a lower C_D, since end effects would exert a greater influence. The difference in C_p on the front of the building and on the rear is clearly less near the ends than at the center. Thus a lower aspect ratio L/H implies a lower drag coefficient C_D. This effect is corroborated by the extensive experimental results of Wieghardt (1953). Figure 4 shows that increasing L/H increases C_D for models of square cross section. The reference velocity U_R used in Fig. 4 is the integrated average in the range $0 < y < H$.
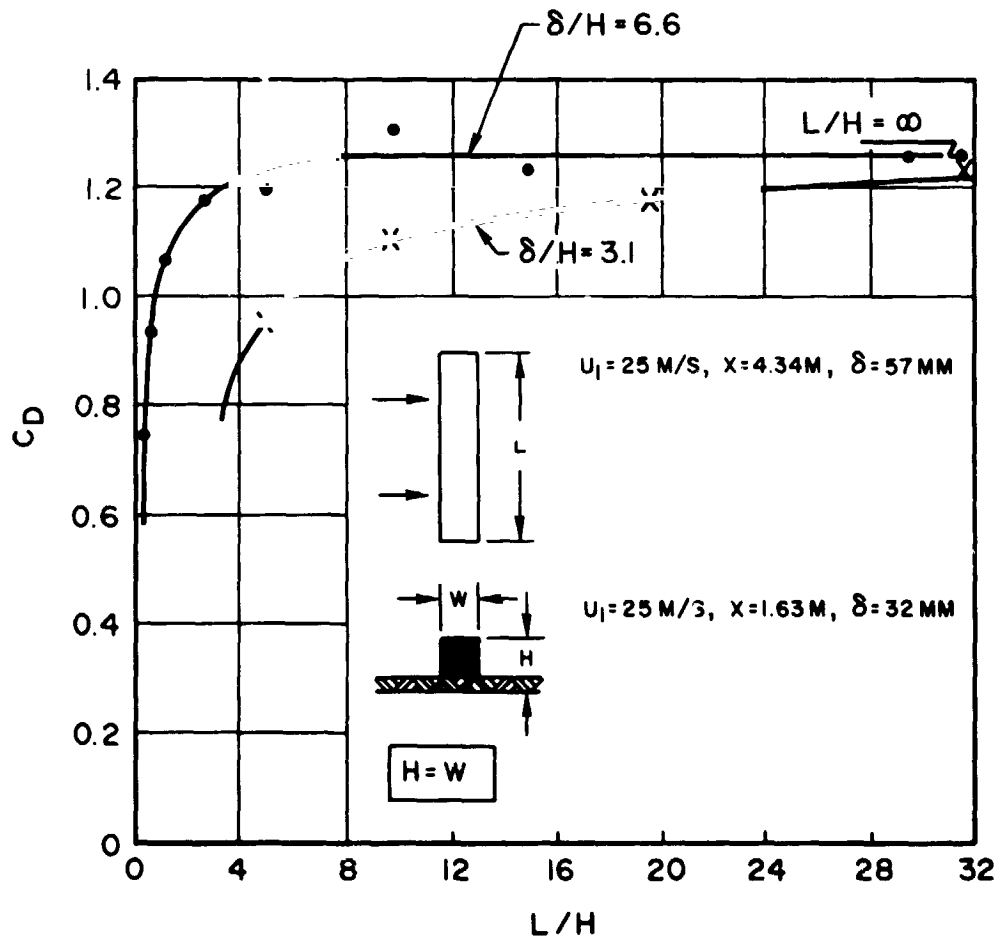
Fig. 4. Measurements of Wieghardt (1953) Showing the Effect of L/H and δ/H on C_D

9

Wieghardt's results show that C_D increases with H/δ and with $U_RH/$
The ratio of H/W, model height to streamwise width, also affects C_D.
Fence-like models with large values of H/W have the highest drag coeffi-
cients. Similarly the cross-sectional shape of the model affects C_D.
Profiles having a sharp edge at the roof line have the highest drag
coefficients.

Referring to (1.1) it is observed that all the terms on the right-
hand side are affected by a change in C_D, except the first term, which
depends on the upstream profile. The second term is affected most
substantially and will decrease with an increase with C_D. This term
represents the major part of the momentum flow from the control volume.
Measurement of centerline velocity profiles and evaluation of $\int U^2 dy$
provides a measure of this term, and changes in this integral are pro-
portional to changes in C_D. Wake velocity profiles are thus related to
the geometical features of the flow through (1.1) and (1.2). The
momentum flux at the centerline can be obtained from velocity
measurements of the present work.

CHAPTER 2

EXPERIMENTAL WORK

1. Models

Block-type buildings were modelled using sections of square
aluminum bars which were cut to several lengths. The height H of the
models was 8.38mm ± 0.01mm, and the streamwise width W was likewise
8.38mm. The length L of the models was equal to 3H, 6H or 9H.

For multiple-building arrays, the space S is also varied. Figures
5-9 depict the arrangements studied and indicate the notation mentioned.
All lengths are even multiples of the model height H.

The models were mounted in arrays on the floor of the wind tunnel
and securely glued in place. The arrangements used are indicated in
Table I. The infinite spacing (S = ∞) refers to the single building as
shown in Fig. 5. The lateral spacing, where buildings are separated
laterally, is always 6H.

2. Wind Tunnel

Figure 10 is a schematic depiction of the wind tunnel used for the
model tests. Room air was drawn into the tunnel through a filter, and a
boundary layer was developed on the floor between the inlet and the test
section. The models were mounted 4.88m from the inlet, which left 2.44m
of tunnel length downstream of the models.

The floor of the tunnel is 56 cm wide and is made of plywood
covered with a layer of Formica. The sides and roof are constructed of
Plexiglas. The roof was adjusted to give a zero pressure gradient flow,

11
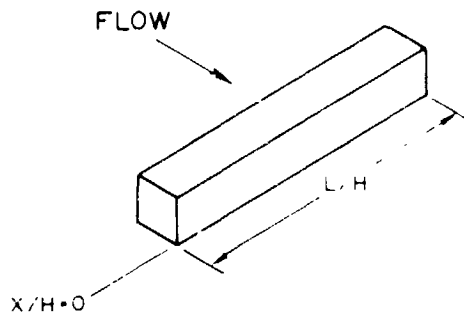
Fig. 5.Single-building Model Arrangement with Variable L/H
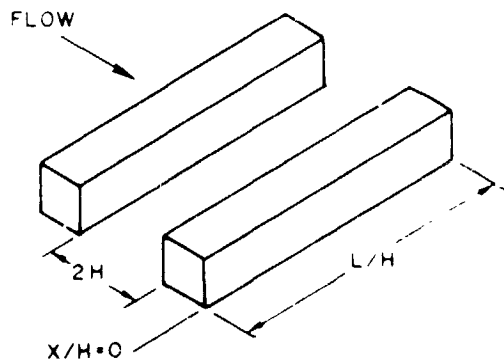
Fig. 6.Two-building Model Arrangement with Variable L/H
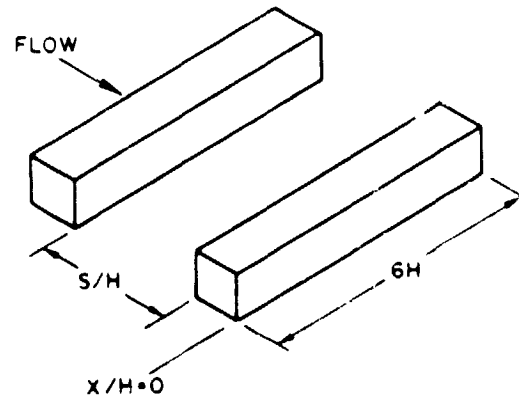
Fig. 7.Two-building Model Arrangement with Variable S/H

12

FLOW

6H

S/H

X/H = O
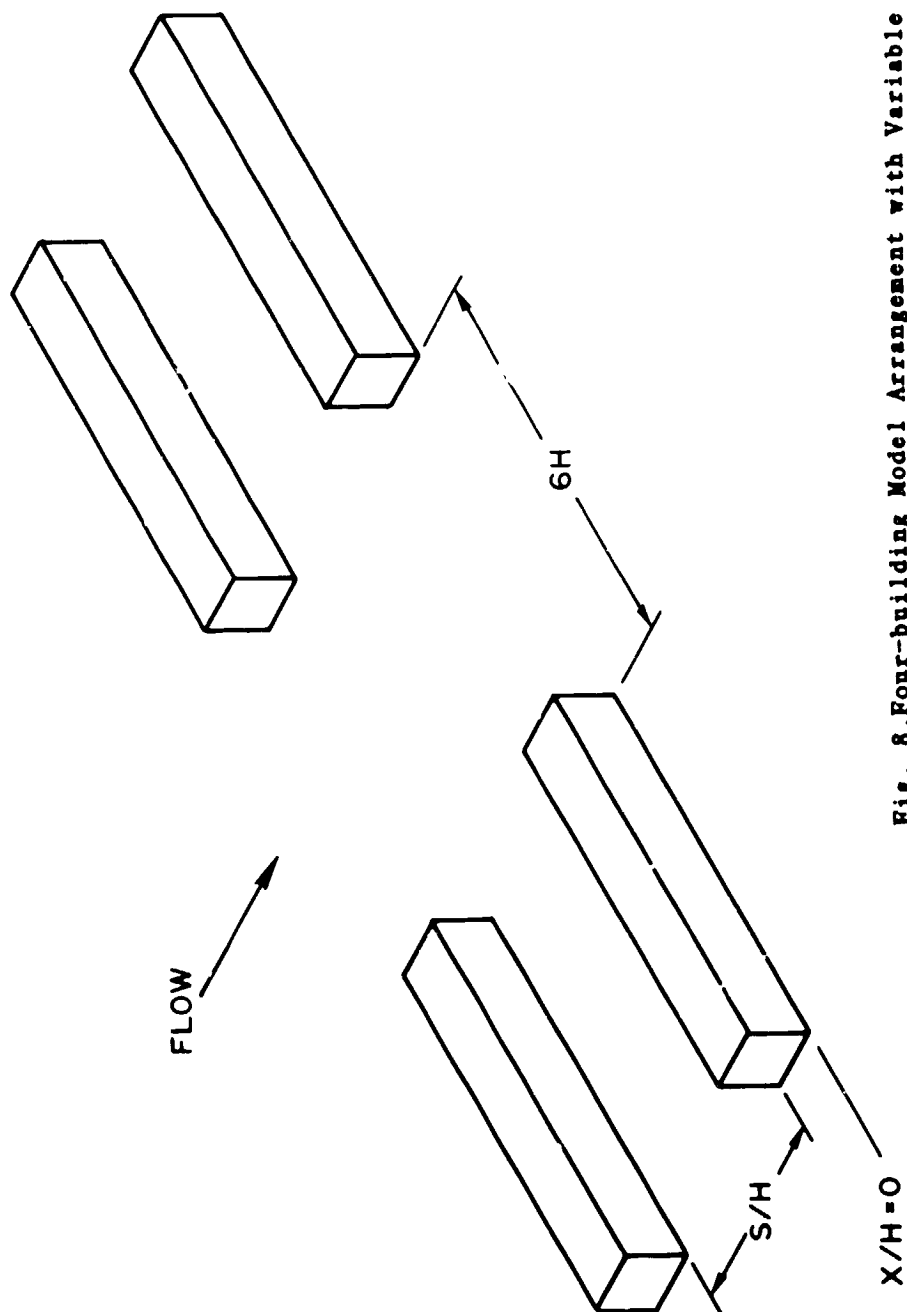
Fig. 8. Four-building Model Arrangement with Variable S/H

FLOW

6H

S/H

X/H=O
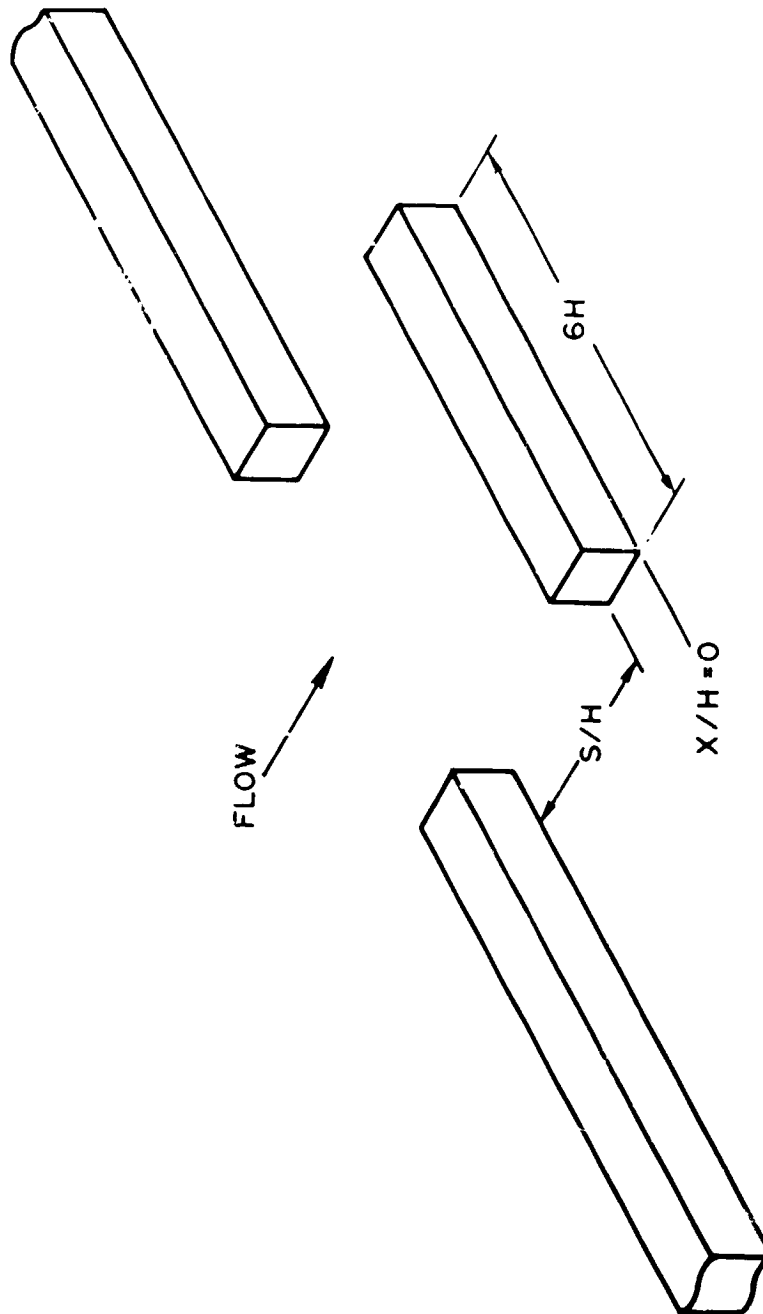
Fig. 9. Three-building Model Arrangement with Variable S/H
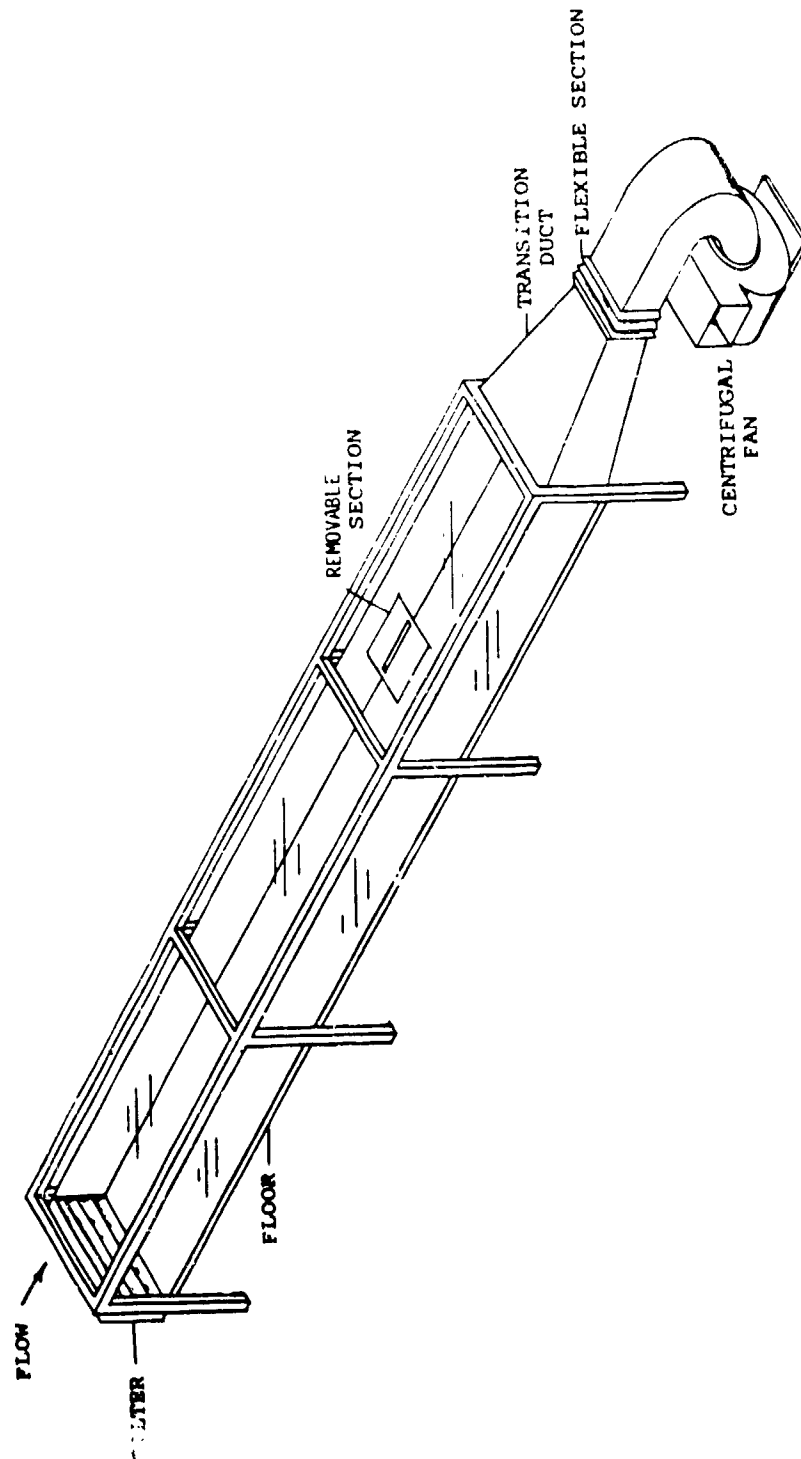
Fig. 10. Schematic of Wind Tunnel

15

and its height above the floor varied from 25.4 cm at the inlet to 29.9 cm at the exit. Pressure taps in the sides of the tunnel were used to determine the required adjustment of the roof.

The roof was slotted to allow the insertion of probes, but the slots were covered during tests to assure minimum leakage. Probes were supported and moved by a traversing carriage, which allowed probe movement in three directions.

TABLE 1

Building Arrangements

Pattern No.	Shown in Fig. No.	Length L	Spacing S
1	5	6H	∞
2	6	6H	2H
3	5	3H	∞
4	6	3H	2H
5	7	6H	3H
6	7	6H	6H
7	7	6H	9H
8	5	9H	∞
9	8	6H	3H
10	8	6H	6H
11	8	6H	9H
12	9	6H	3H
13	9	6H	6H

A tripping rod and a section of sandpaper on the floor near the inlet of the tunnel was used to promote rapid development of a boundary layer. The thickness of the boundary layer formed on the floor of the tunnel at the position of the models (x   4.8m) was approximately 10H. The freestream velocity U_1 at this point was maintained at $6.7 \pm .1$ m/s. The temperature of the air in the room, which was drawn into the tunnel, was controlled to 25 ± 1 degrees Celsius. Under these conditions the obstacle Reynolds number, defined as $U_i H/$, was approximately 3750.

3.   Flow Visualization

The adaptation of the oil-film technique to visualize surface flow paths by Logan and Lin (1982) was applied to all of the model arrays in Table I, except for pattern nos. 2 and 4. A mixture of isopropyl alcohol and charcoal powder (0.567g charcoal/55 ml alcohol) was poured over the floor of the tunnel immediately around the models. Photographs were taken just after the first 15 seconds of tunnel operation. All photographs were made with a tripod-mounted 35mm camera supported above the roof of the test section. The camera setting used was f/5.6 and 1/125 sec. The film used was Tri-X ASA 400, and prints were made on high contrast F5 photographic paper.

4.   Measurements

Preliminary measurements of the three components U, V and W of mean velocity in the wakes of pattern numbers 1 and 6 (Table I) were obtained with a three-dimensional Pitot tube. This probe was the model DC-125 directional probe manufactured by United Sensor and Control Corporation. The probe connections were made as shown in Fig. 11. The pressure

17

PITOT TUBE

P_{ATM}

VALVE
MANIFOLDS

MANOMETER

PRESSURE
TRANSDUCER

0 000

BRIDGE
AMPLIFIER

VOLTMETER
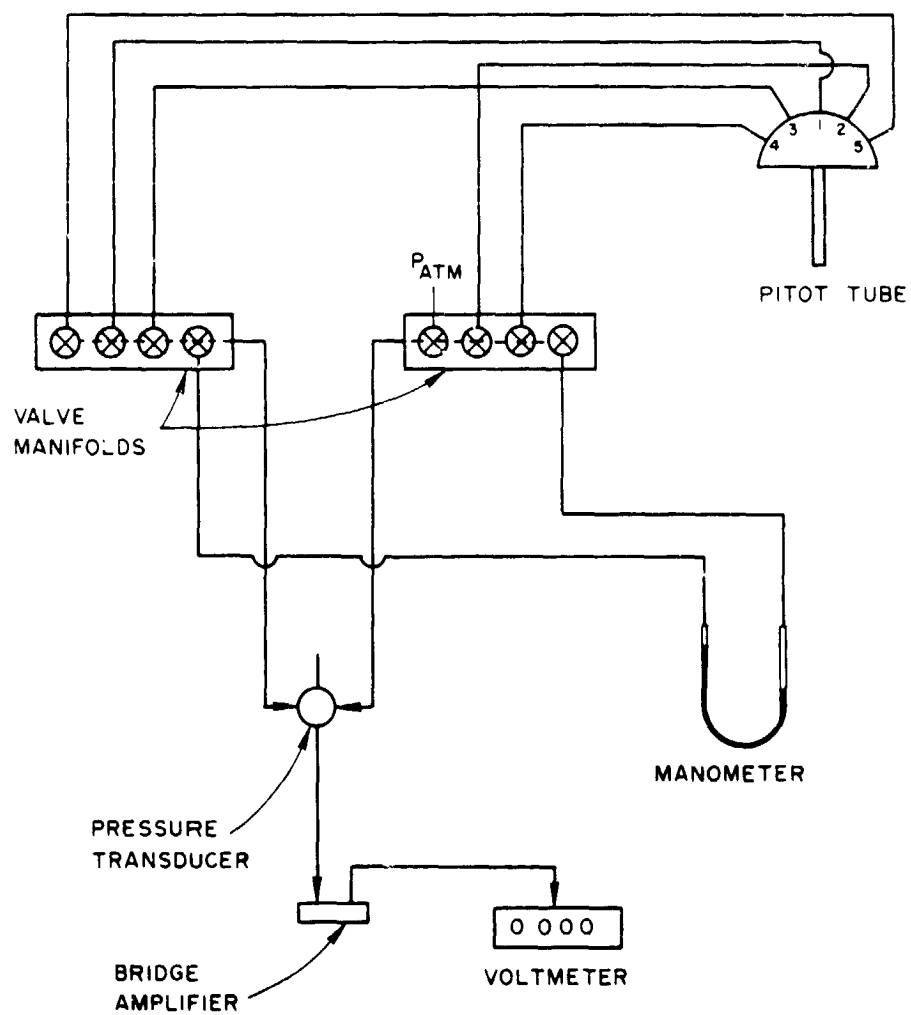
Fig. 11. Directional Probe Connections

transducer was a Gould-Statham Model PM5 (0.3psid), and the bridge amplifier was a Fogg model 50.

The pressure probe permitted the making of off-centerline measurements but was not useful for detailed measurements very near to the floor. Thus profiles of mean velocity U and root-mean-square fluctuation u' were carried out at centerline stations for all building arrays listed in Table I using a single-, normal-rod TSI 1210-20 hot-film probe of 0.0508mm diameter. Detailed mean velocity and turbulence intensity profiles were obtained with this probe. The TSI 1050 series instrument used with this probe comprises four parts: a 1050 Constant Temperature Anemometer, a 1051-6 Monitor and Power Supply, a 1072 Signal Linearizer and a 1076 True RMS Voltmeter. A DISA 55D35 RMS unit was also used to measure the RMS values.

Since a typical sensor (TSI 1210) was used in an air flow of low velocity range (0-30 fps), the four polynomial coefficients involved in the adjustment of the linearizer could be obtained from the manufacturer-supplied Table of Coefficients. Because the freestream velocity U_1 was used as a non-dimensionalizing quantity, the non-dimensionalized values of mean and fluctuating velocities were really just relative values to that of U_1, so the only calibration needed was to secure a consistent freestream velocity value. The Linearizer was set to give a velocity reading of 10 volts when the probe was moved to a reference position in the freestream. The readings of mean and fluctuating velocities which were recorded were already non-dimensionalized.

CHAPTER 3

SURFACE FLOW AROUND MODELS

Figures 12-15 show photographs of streak patterns formed with the alcohol-carbon powder mixture on the floor of the wind tunnel in the vicinity of the models. Most of the arrays listed in Table I were studied in this way. The photographs give useful information about the extent of the disturbance to the flow field around the models. Noting that the squares of the superimposed grid are 2H in size, it is observed that the flow field is influenced to a distance of about 6H away from any side of the block-type model.

The asymmetry of the upstream flow patterns is evident in Figs. 12-14. Although the models were set at approximately 90 degrees to the side walls of the tunnel, it appears that some small deviation from 90 degrees must exist between the velocity vectors of the upstream particles and the models. This may be explained by a small lateral component of mean velocity, which produces an angle between the velocity and the models of slightly less than 90 degrees. Such a lateral component is expected, when turbulent boundary layers are developing in non-circular ducts. For example, Pletcher and McManus (1965) reported secondary currents as high as one percent of the freestream velocity. Logan and Lin (1982) reported secondary currents in the wind tunnel used in the present investigation. Apparently the slightest deviation from a 90-degree direction of the velocity vector shifts the stagnation region noticeably. The smoke-filament studies of Holdredge and Reed (1956), shown in Fig. 16, also indicate that the stagnation point shifts to a
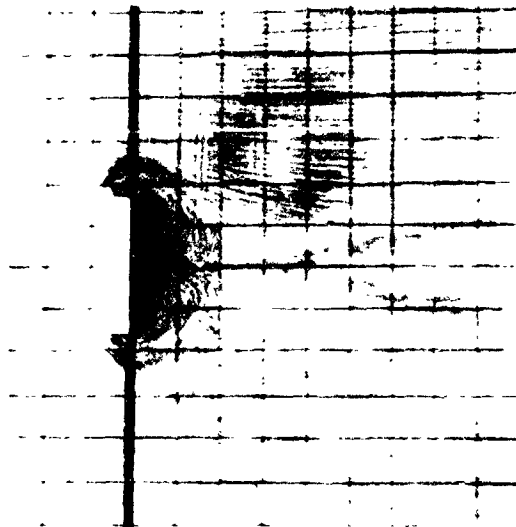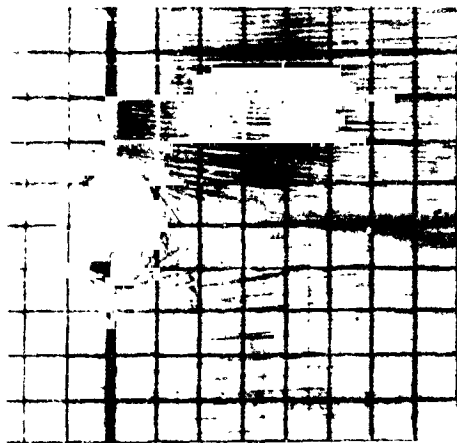
Fig. 12. Surface Flow around Single Buildings

21
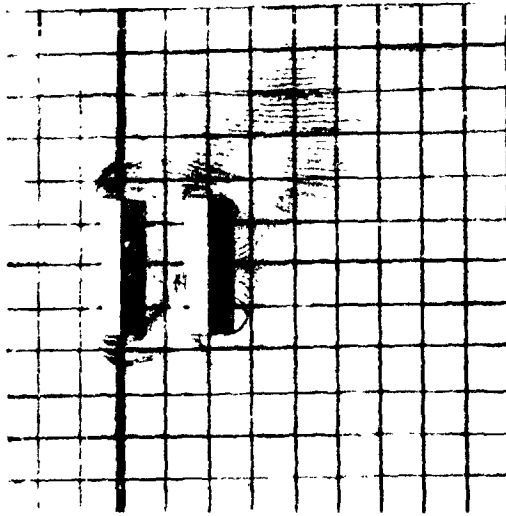
S = 3H
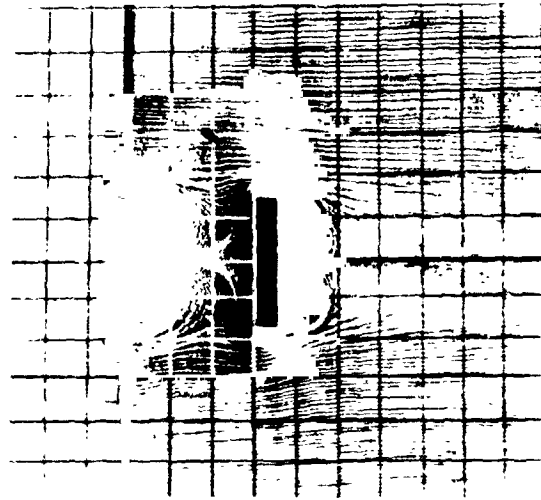
S = 6H
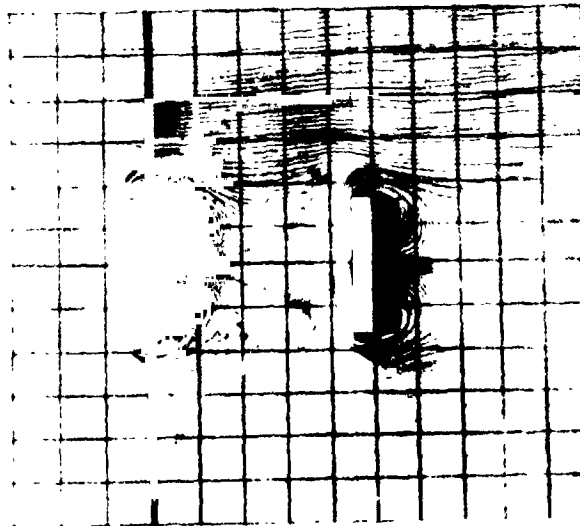
S = 9H

Fig. 13. Surface Flow around Buildings in Tandem

S = 3H

S = 6H

S = 9H
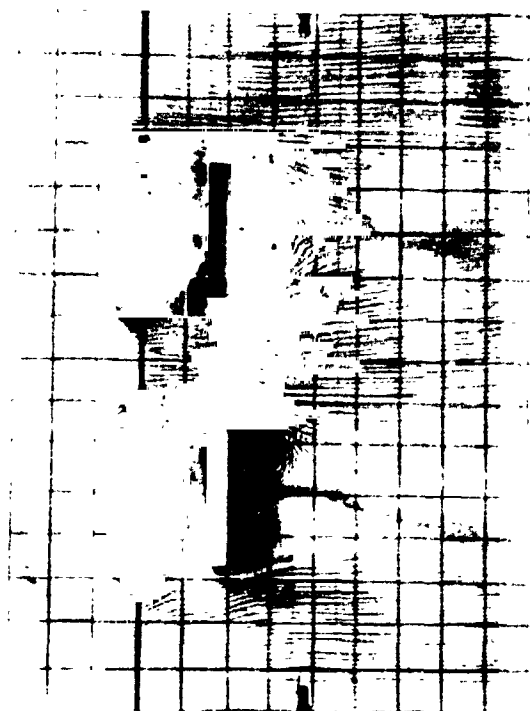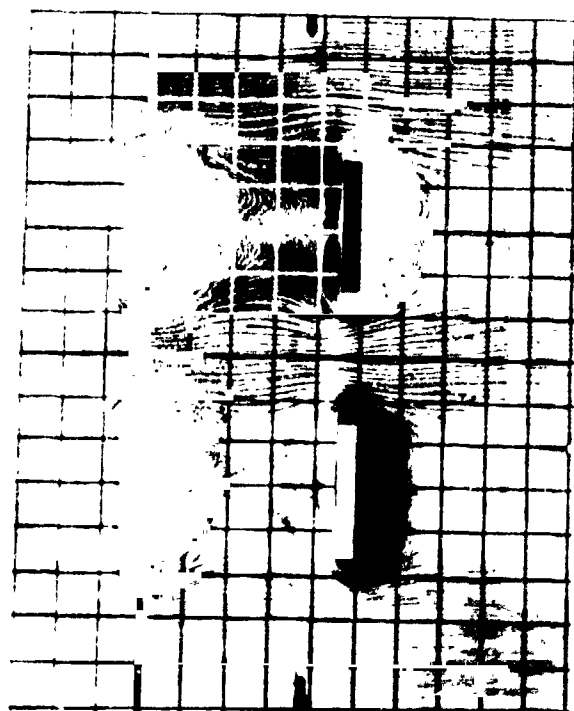
Fig. 14. Surface Flow around 4-building Arrays
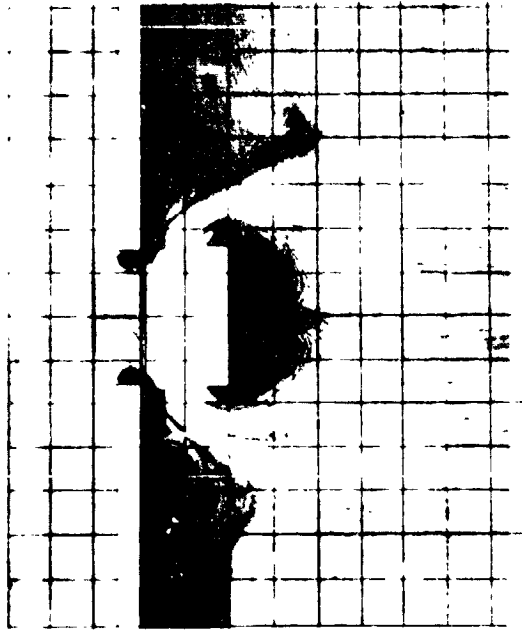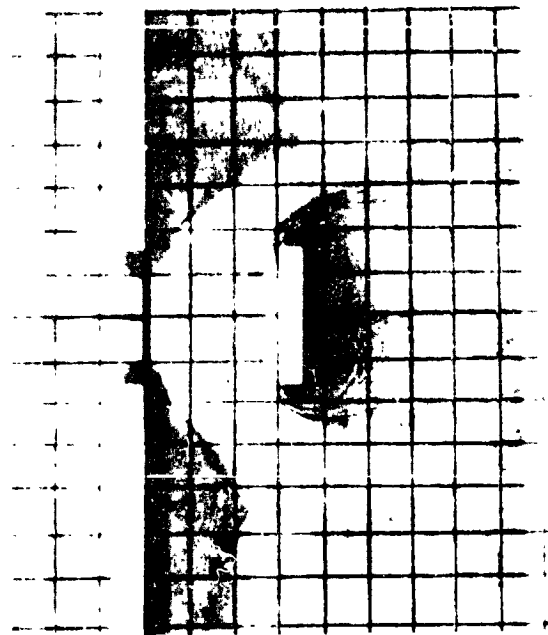
Fig. 15. Surface Flow around 3-building Arrays
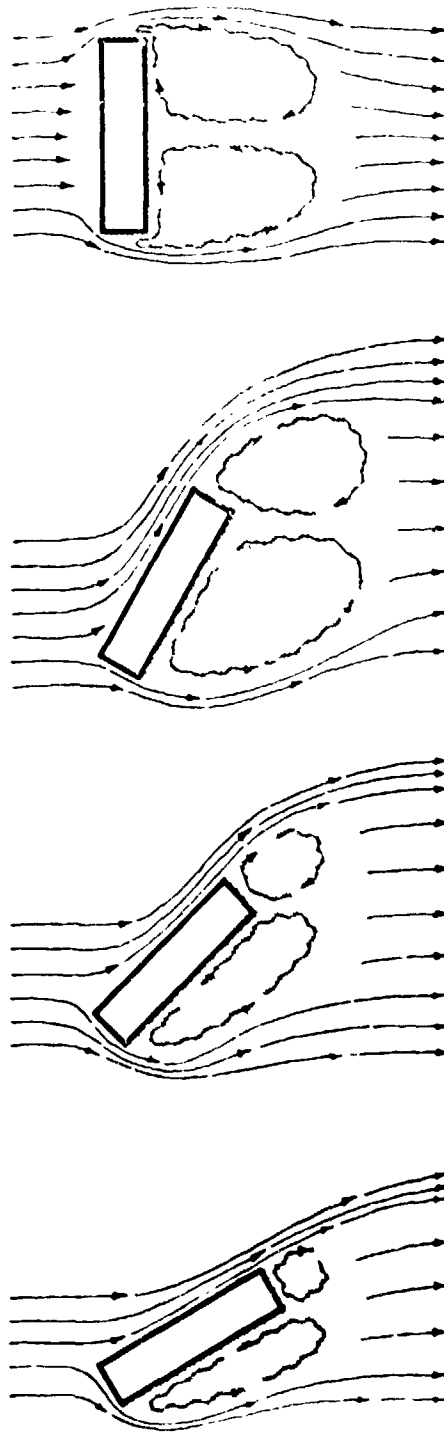
Fig. 16. Streamline Patterns from Smoke Studies of Holdredge and Reed (1956)

position near the leading corner of a model in a skewed position with respect to the approaching stream.

The surface flow pattern around the single model, shown in Fig. 12, shows symmetrical flow fields in the recirculation zones behind each of the three buildings tested. Fluid from the end regions passes into the region behind the buildings and approaches the back sides near the centerline, as shown in Fig. 1. The line which divides building-directed fluid from downstream-directed fluid is curved and reaches a maximum distance from the back side of the model on the centerline. This reattachment distance is approximately 3H, 5H and 7H for the models of lengths 3H, 6H and 9H, respectively. These distances agree quite well with those given by Holdredge and Reed (1956), as taken from the graph in Fig. 1, except for the longest building. The graph of Fig. 1 for W/H = 1 is a reasonable representaion of the maximum dimension of the recirculation region, although it could be modified slightly by the present results.

The contrasting dark and light areas in Fig. 12 are assumed to indicate regions of low and high surface shear stress, respectively. There are, of course, inconsistencies, e.g., shadows, such as the dark annular region caused by the lamp used for lighting the test section. The separation regions at the sides and back of the models are darker, and the stresses there are low. Along the centerline downstream of the recirculation region, there is a dark, wedge-shaped region. In this section of the wake, the surface stresses and low-level velocities are low. Fluid moves from the two adjacent sides into this region, and the central region increases in velocity and shear stress at the expense of the regions on each side of it. Thus the wake of low-momentum fluid

26

spreads in a wedge-shaped manner. The half-angles of the wedge-shaped areas are approximately 7, 14 and 18 degrees for models of length 3H 6H and 9H, respectively. The virtual origins of wedges appear to be located approximately at distances of 8H, 4H and 2H downstream of the back side of the models of lengths 3H, 6H and 9H, respectively.

Figure 13 shows the effect on the flow field of a tandem arrangement of two identical buildings. The shortest spacing S is 3H. For this case the flow field does not appear to develop in the rear of the first building. Instead the flow develops around both buildings as a unit, and the recirculation region formed behind the second building is like that for a wide building, i.e., W/H > 2. In Fig. 1 the W/H > 2 curve indicates a reattachment length of 3.6 H. This is in good agreement with the observed value for S = 3H in Fig. 13. Figure 13 shows a recirculation zone behind both buildings when the separation is 6H and 9H. However, the reattachment length behind the second building is only about 4H for the largest separation, whereas it is closer to 5H for the single-building case. The wedge-shaped region is also present with the tandem arrangement, and the half-angle of the wedge is roughly the same as behind the single building. However, the virtual origin of the wedge is somewhat closer to the back side of the model.

The wedge locations for the arrays of Fig. 14 are slightly different from one another, although the tandem arrays are identical. Otherwise the flow patterns are individually very similar to those in Fig. 13. If the wedge patterns define the region of retarded fluid, the approximate location of the intersection of the neighboring wedges should correspond with the point of maximum retardation and should be observable from centerline velocity profiles. For a 15-degree

27

half-angle of the wedge and with the 6H lateral separation shown in Fig. 14, calculations results indicate a wake intersection at 24H.

The recirculation zone for a building located behind the gap between two long buildings is shown in Fig. 15. The reattachment lengths for these cases are close to those of the single building in Fig. 12, i.e., they comply roughly with the graph of Fig. 1. Because the flow behind the downstream building is bounded at either side by retarded fluid from behind the long, upstream buildings, there is less interaction, and apparently no wedge-shaped region is formed. The gap flow upstream is disturbed considerably by the model behind the gap. The flow through the gap is probably reduced in the central region by the obstacle, with a resulting increase in flow above this region, but the flow between the ends of the buildings may be intensified, at least for the spacing of 3H, as indicated by the light areas at the ends of the central building.

CHAPTER 4

VELOCITY PROFILES

1.   Upstream Profiles

Profiles of mean velocity and turbulence intensity taken with no models on the floor of the tunnel are shown in Figs. 17 and 18, respectively. These profiles wei taken wit 'he hot-film probe described in Chapter 2. The honeycomb flow straightener was removed for this test and for all hot-film measurements reported in the chapter. The profiles are compared with those previously reported by Logan and Barber (1980), using the same tunnel geometry, but with the tunnel located in a different room. A difference in shape of the velocity profile is noticeable. The free stream turbulence level in the new location is significantly higher. Apparently turbulence generated outside the tunnel is more significant in the new tunnel location, and the root-mean-square of the longitudinal fluctuation u' amounts to 4.9 percent of the free stream velocity U_1.

The effect of an increase in the high free stream turbulence intensity on the mean velocity profile is to lower the shape factor H (defined as the ratio of displacement thickness to momentum thickness). The change of velocity profile, corresponding to a change of H, shown in Fig. 17 agrees with that predicted by McDonald . ' Kreskovsky (1974).

2.   Wake Profiles

Wake Profiles of mean velocity were measured downstream of the patterns described in Table I. Measurements wei. made at stations which

29
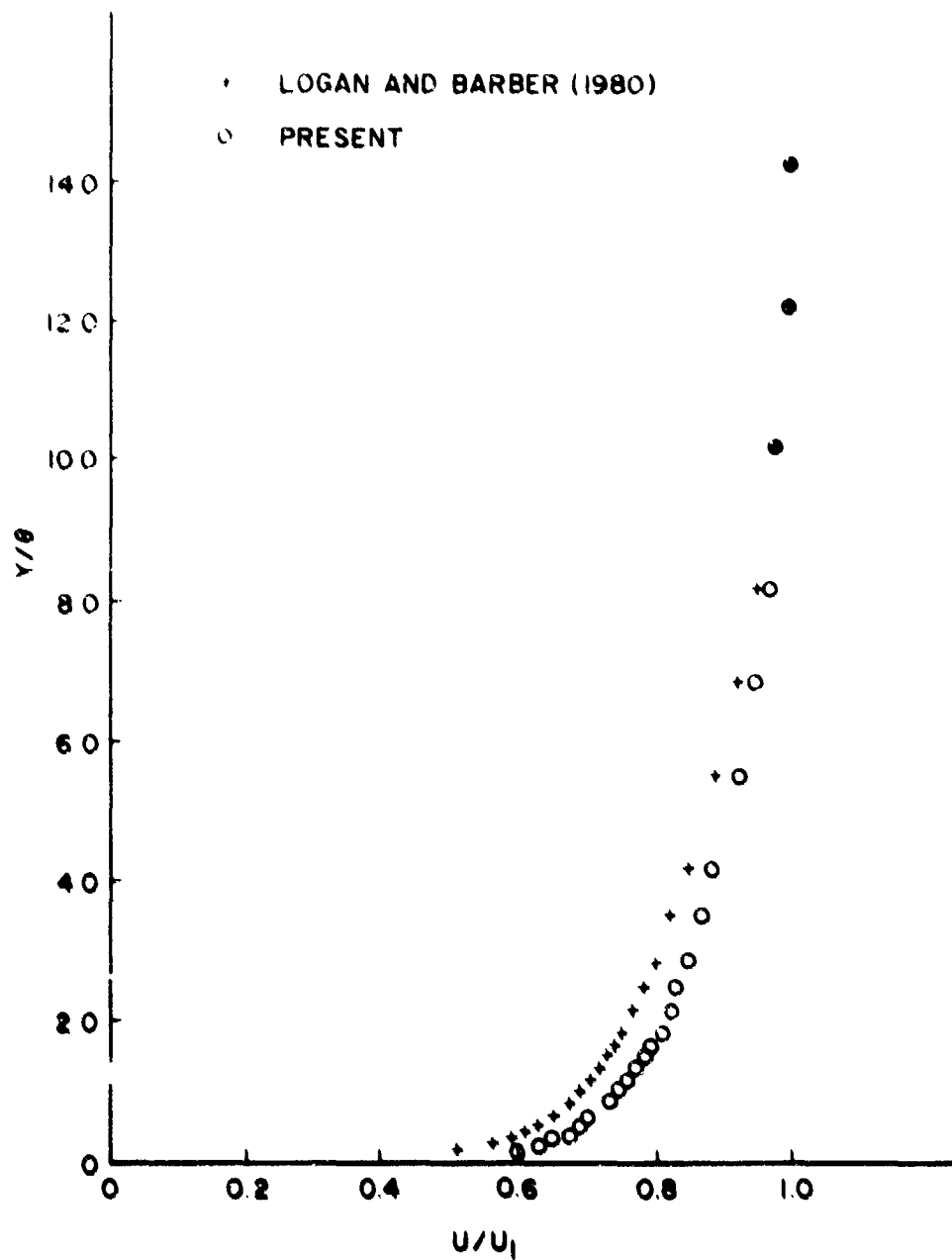
Fig. 17. Velocity Profile Upstream of Models
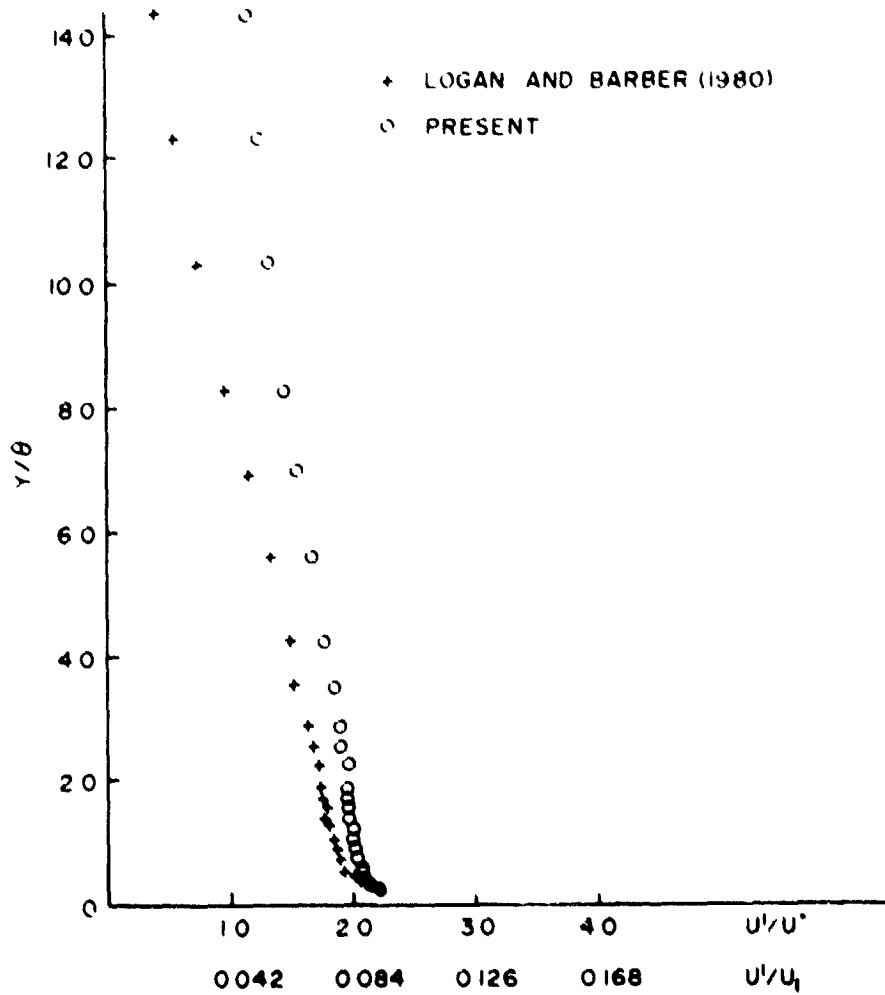
Fig. 18. Turbulence Intensity Upstream of Models

were located at distances of 2H, 4H, 6H, 10H, 16H and 28H from the rear (downstream) side of the building model. The earliest measurements were made in the wakes of pattern nos. 1 and 6 (Table I) using a five-hole-pressure probe. These measurements are presented in the Appendix in Tables A-1 to A-6.

The pressure-probe measurements are useful in that the three velocity components U, V and W are given. They serve as a means of constructing a qualitative flow picture in the wake behind the single building (L = 6H) and the two-building, tandem array (both buildings have L = 6H). These data should be considered only qualitative, as good accuracy is precluded by the relative size of the probe (3.175mm diameter) as compared to the height of the model (H = 8.38mm) and to the thickness of regions of high velocity gradient generated behind the models.

Measurements of wake profiles of mean velocity (longitudinal component U) and turbulent fluctuations (rms of longitudinal component) were made behind all 13 patterns of Table I using the hot-film probe. Since the sensor for this probe (TSI 1210) is a cylinder 0.0508mm in diameter and is held parallel to the floor and normal to the main flow direction (x-direction), detailed wake measurements in the region of high velocity gradient were feasible. Profiles measured with the hot-film probe were obtained only at stations on the centerline, however. At the centerline the measurements of mean velocity include a vertical component V as well as the horizontal component U. Since the angle of the resultant velocity vector is not determinable with the single-sensor, normal, hot-film probe, the effect of the vertical component is ignored in this report. The worst error due to this effect is expected to be 1 to 1.5

percent and would occur close to the model, say in the region bounded by $o < y/H < 3$ and $o < x/H < 10$.

Preliminary Velocity Measurements: Pressure Probe Results

The data of Table A-1 to A-6 were taken with the five-hole pressure probe. The results are given to aid in building a qualitative picture of streamlines at various levels in the wake region. In the wake of a building arranged as in Fig. 1 a low speed region of reversed flow is expected to occur just behind the building. The flow around the sides and roof of the building is accelerated initially but later mixes with and accelerates the retarded fluid directly downstream of the building. Near the surface (floor of the tunnel) the velocity profiles show increases in U/U_1, as x/H increases. The increase in U at low levels in the central wake region means that mass must be added to the region from regions above or to the sides of this region. Tables A-2 and A-3 show that $V < 0$ and $W > 0$ at all off-centerline stations in the wake of the single building. Flow occurs towards the centerline and towards the ground (floor of the tunnel) in the wake region. The same general features of the wake flow are observed in the data of Tables A-5 and A-6, which were obtained behind two buildings in a tandem array.

The relative magnitudes of the vertical velocities, given in Tables A-2 and A-5, are of interest in the determination of aircraft response during flight through building wakes. A low-level flight through a wake might be as depicted in Fig. 19. The aircraft would have gained a height above the ground of roughly $y/H = 2$ when it was 10 building heights ($x/H = 10$) to the rear of the building. The downdrafts V from Table A-2 can be used to estimate the deviation of the angle of attack,

33
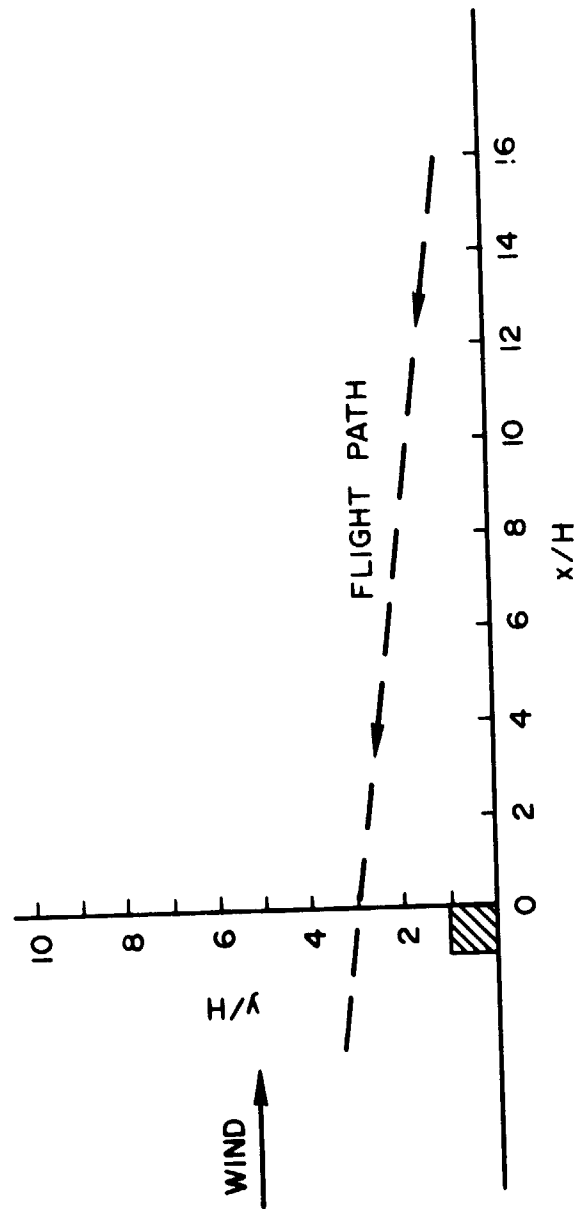
Fig. 19. Aircraft's Path during Takeoff
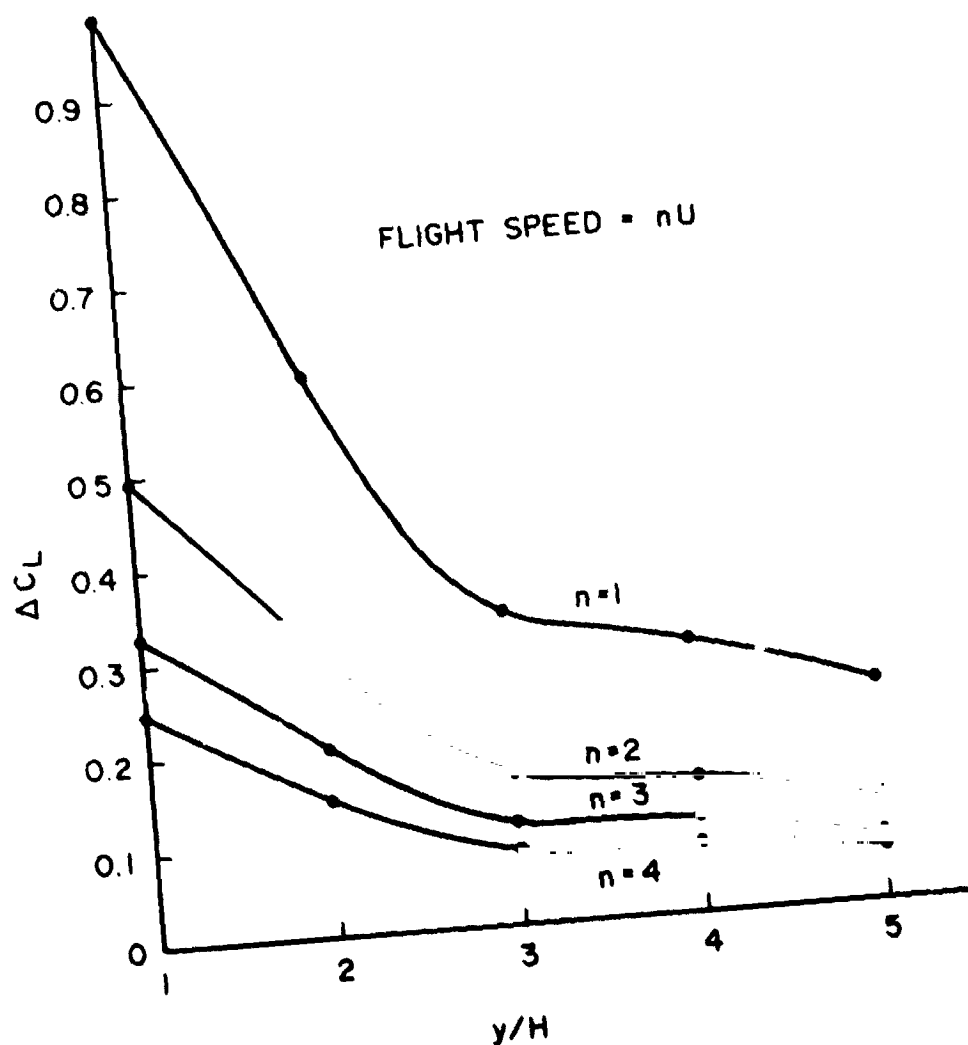
Fig. 20. Change in Lift Coefficient with Downdraft in Single-building Wake at x/H = 10

35

or the lift coefficient C_L, from its value in a purely horizontal wind. This deviation of C_L, denoted by ΔC_L, is plotted in Fig. 20 using the data obtained on the centerline behind a single building at $x/H = 10$. To obtain the values of ΔC_L used in Fig. 20, it is assumed that the deviation of angle of attack $\Delta\alpha$ from the angle of attack α of the wing of the aircraft flying in a horizontal wind is given by arc tangent $[V/(U + nU)]$, where nU is the flight speed of the aircraft. If the flight speed is very low, or the wind speed U is very high, then it is plausible that $n < 4$. The slope of the lift curve of the aircraft is estimated as 0.1 per degree. Assuming an aircraft lift coefficient of 2 to 3, it is seen from the graphs of Fig. 20 that flight through a wake of a building could entail a momentary lift change of from 2 to 25 percent, owing solely to downdrafts in the wake.

The magnitudes of V in Table A-5 for the tandem arrangement are comparable to those in Table A-2 but show somewhat higher values of ΔC_L for the location considered in Fig. 20. For example, ΔC_L is 42 percent higher at $y/H = 3$ and $x/H = 10$ as compared with the value of ΔC_L behind the single building at the same location.

Detailed Velocity Measurements: Hot-film Results

Mean Velocity profiles obtained at centerline stations in the wakes produced by the 13 patterns (Table I) are shown in Figs. 21-46. The detailed profiles show two bends, which constitute upper and lower boundarys of the disturbed region. The height of the upper bend is denoted by δ_1 and that of the lower bend by δ_s. The variation of δ_1 and δ_s with distance x downstream of the building is significant, in that it delineates the region of the wake which is potentially dangerous to

Fig. 21. Velocity Profiles for Pattern No. 1

Fig. 22. Velocity Profiles for Pattern No. 1

Fig. 23. Velocity Profiles for Pattern No. 2

Fig. 24. Velocity Profiles for Pattern No. 2

Fig. 25. Velocity Profiles for Pattern No. 3

Fig. 26. Velocity Profiles for Pattern No. 3

Fig. 27. Velocity Profiles for Pattern No. 4

Fig. 28. Velocity Profiles for Pattern No. 4

Fig. 29. Velocity Profiles for Pattern No. 5

45

Fig. 30. Velocity Profiles for Pattern No. 5

Fig. 31. Velocity Profiles for Pattern No. 6

Fig. 32. Velocity Profiles for Pattern No. 6

Fig. 33. Velocity Profiles for Pattern No. 7

Fig. 34. Velocity Profiles for Pattern No. 7

Fig. 35. Velocity Profiles for Pattern No. 8

Fig. 36. Velocity Profiles for Pattern No. 8

Fig. 37. Velocity Profiles for Pattern No. 9

Fig. 38. Velocity Profiles for Pattern No. 9

Fig. 39. Velocity Profiles for Pattern No. 10

Fig. 40. Velocity Profiles for Pattern No. 10

Legend

□ x/H = 2

O x/H = 4

△ x/H = 6

Fig. 41. Velocity Profiles for Pattern No. 11
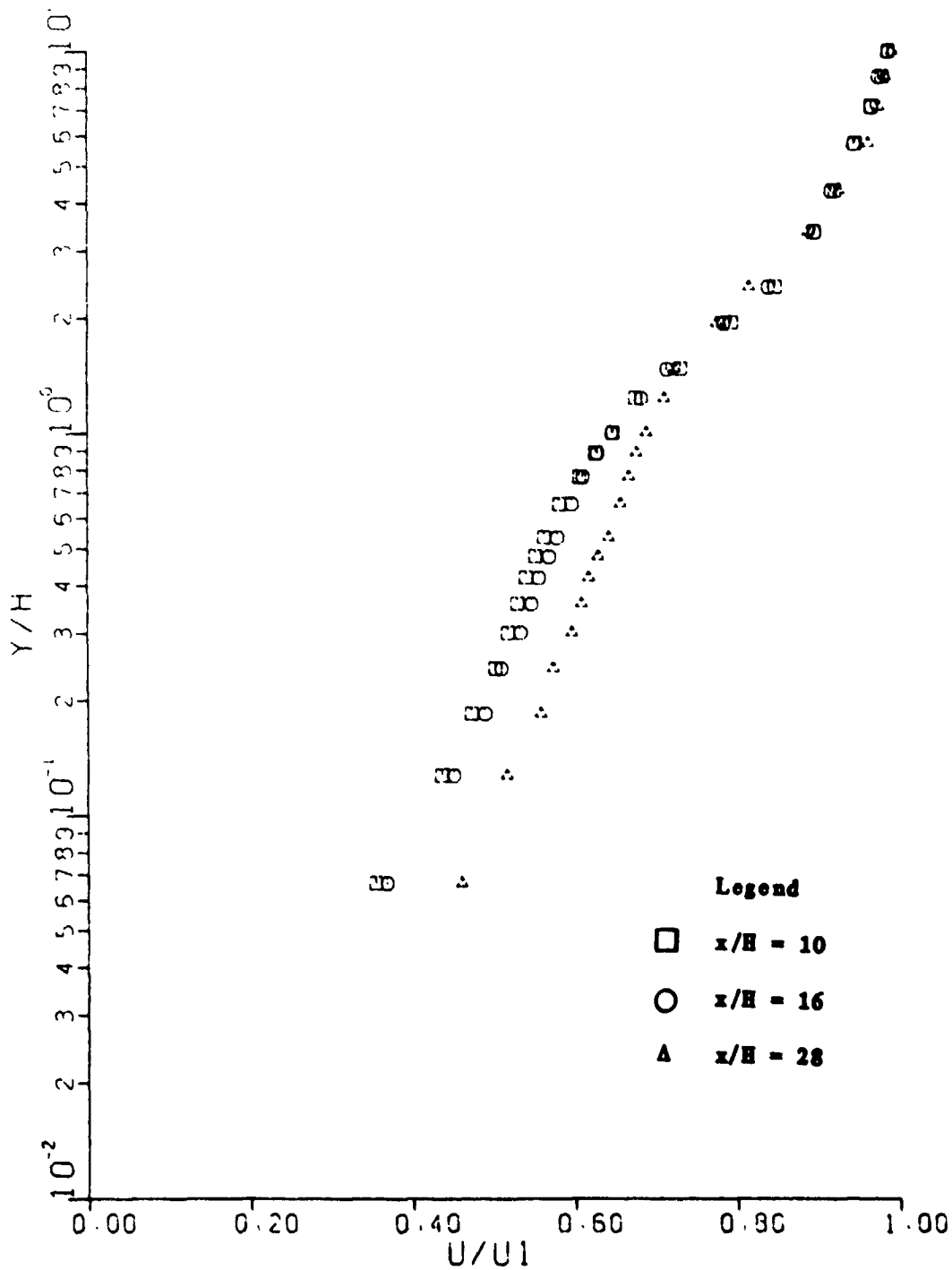
57

Fig. 42. Velocity Profiles for Pattern No. 11

Fig. 43. Velocity Profiles for Pattern No. 12

59
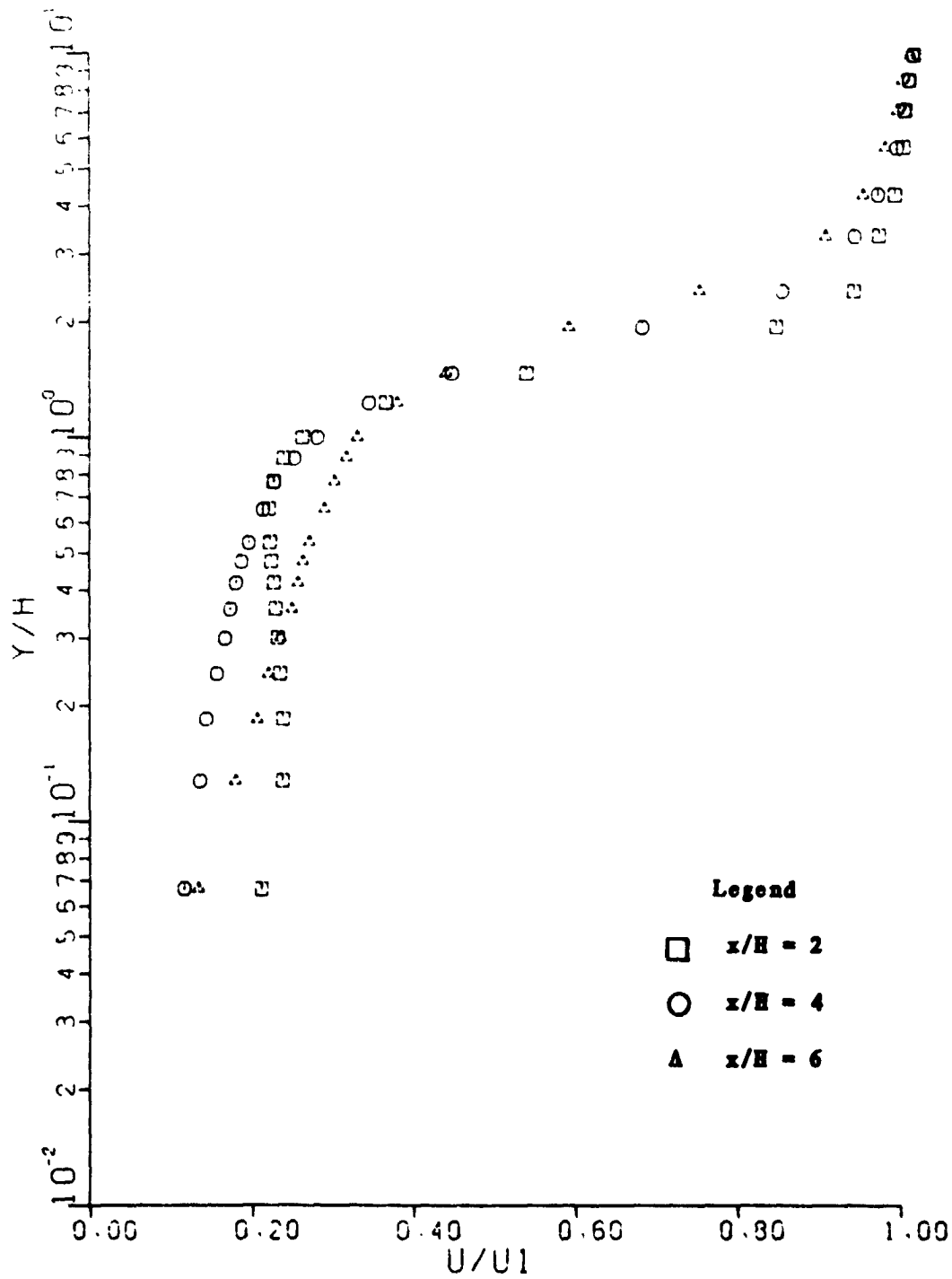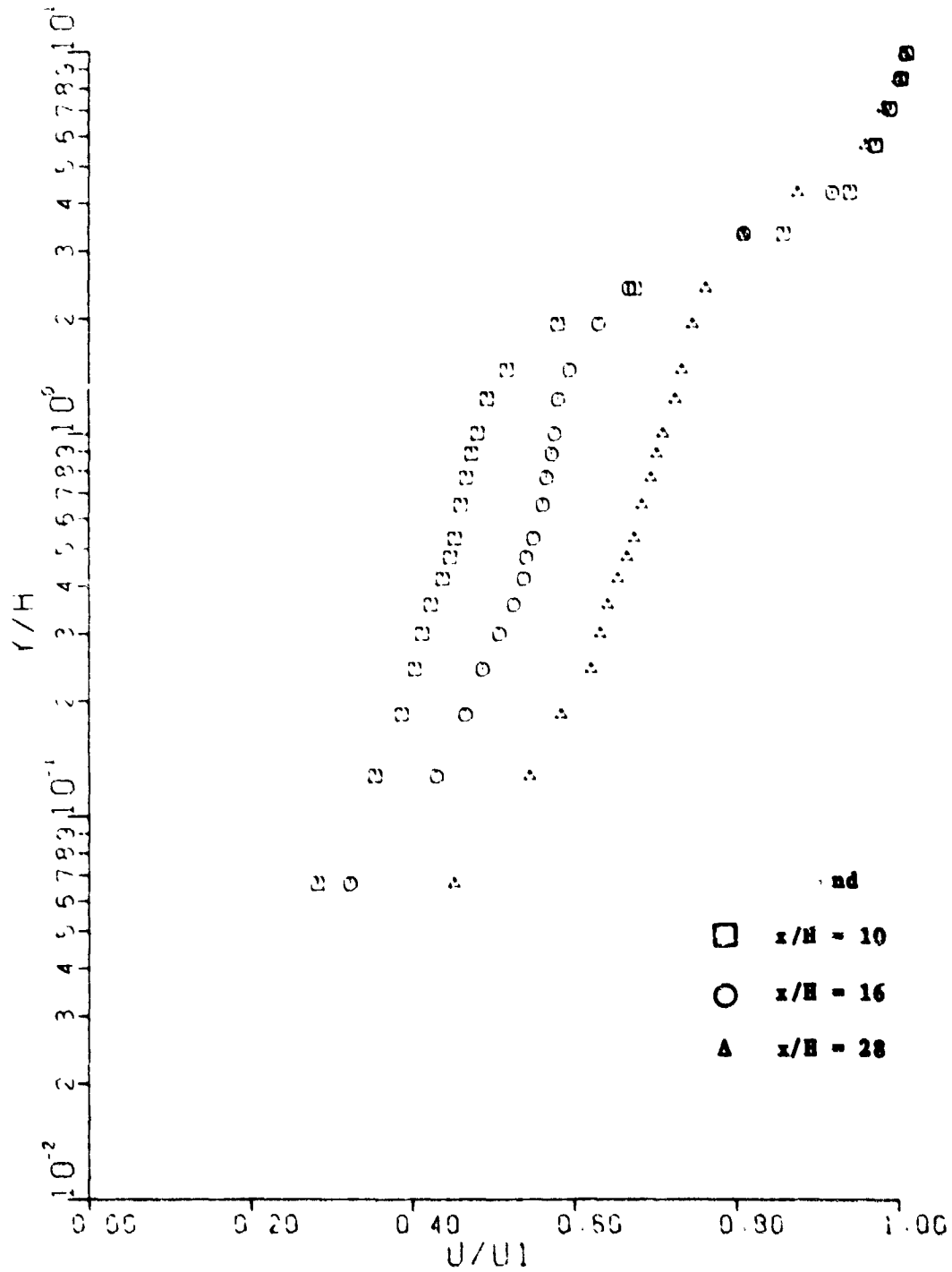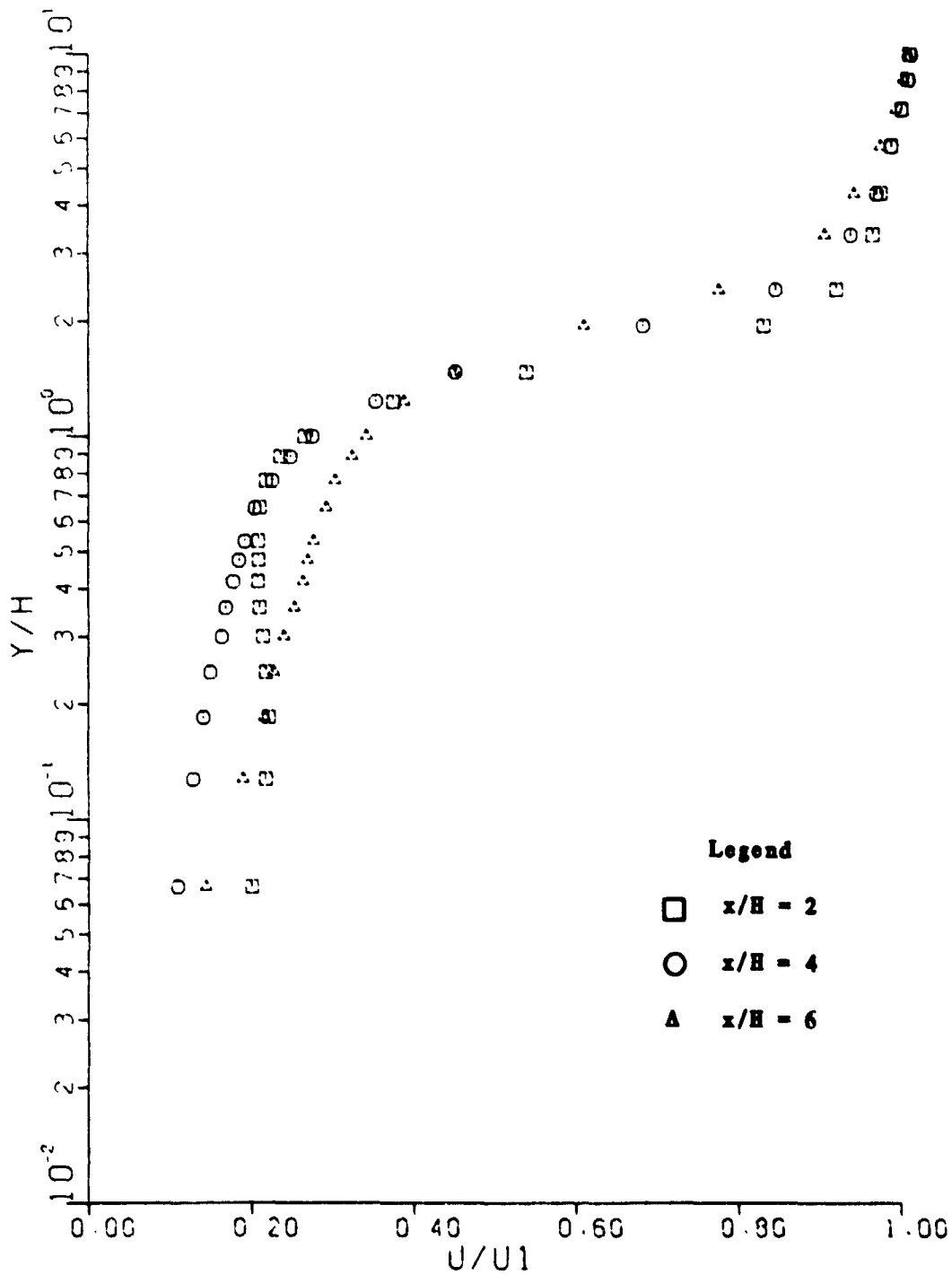
Fig. 44. Velocity Profiles for Pattern No. 12

Fig. 45. Velocity Profiles for Pattern No. 13
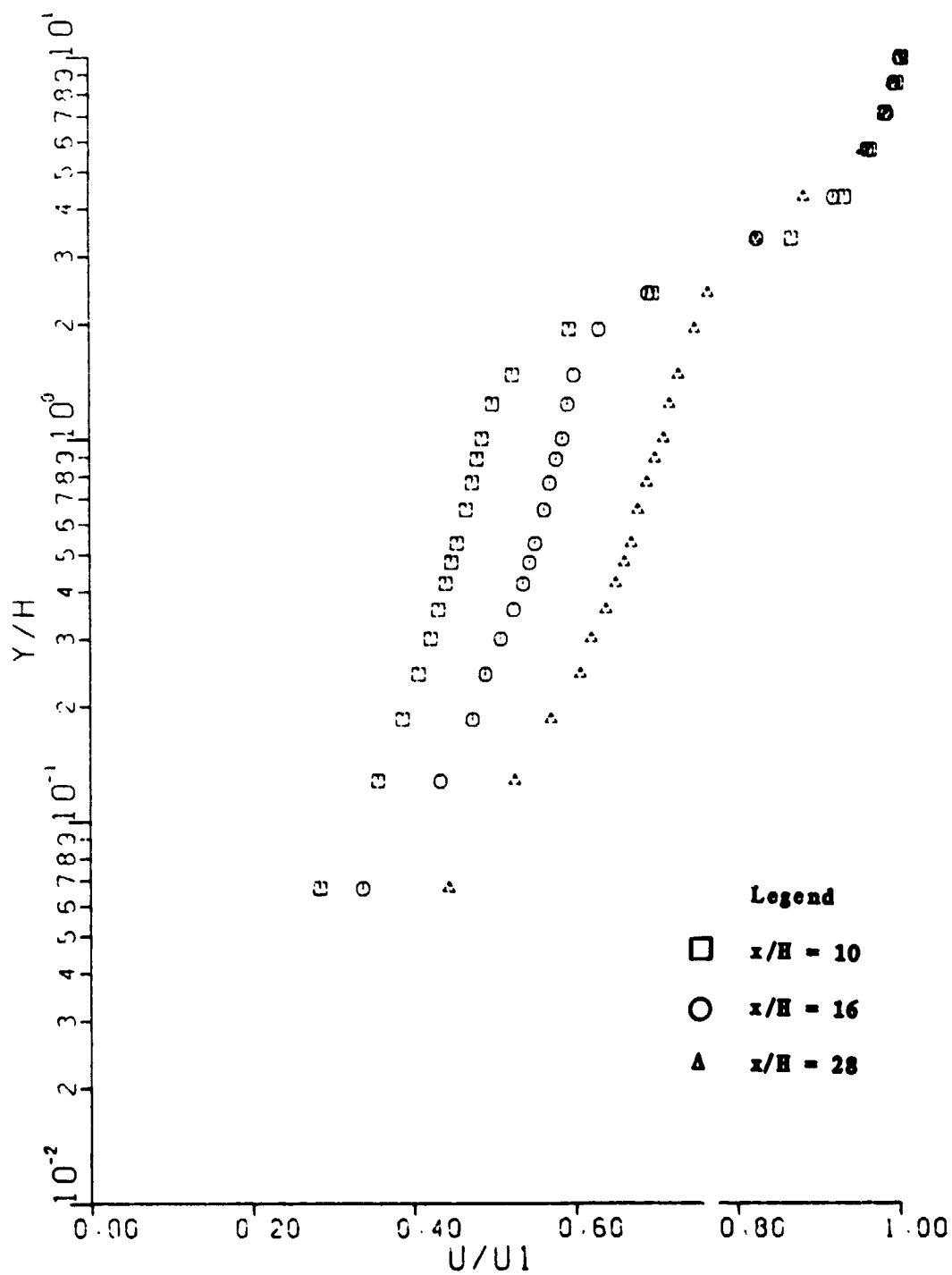
Fig. 46. Velocity Profiles for Pattern No. 13

aircraft. In particular the region bounded by the lower height δ_s and the upper height δ_i is one of high velocity variation, i.e., the velocity gradient dU/dy is higher than found in the undisturbed profile at the same elevations.

The semilogarithmic plots of Figs. 21-46 show that the velocity profile can be approximated by a straight line between the two bends, i.e.,

$$\frac{U}{U_1} = A \ln \frac{y}{H} + B \tag{4.1}$$

is the equation of the straight portion. Thus

$$\frac{du}{dy} = \frac{AU_1}{y} \tag{4.2}$$

and

$$\frac{dU/U_1}{dy/H} = \frac{AH}{y} \tag{4.3}$$

The parameter A is a useful measure of the magnitude of the velocity gradient. For a given straight-line segment, A and B are constants and can be determined from the graphs.

Values of δ_i, δ_s and A were obtained from the graphs and are presented graphically in Figs. 47 and 48 for single buildings and for one tandem arrangement. The data of Logan and Barber (1980) for building of infinite length are included also. The solid curves show the position of δ_i and δ_s, and the area between these curves represents the disturbed region, i.e., the region of higher-than-average dU/dy or A.
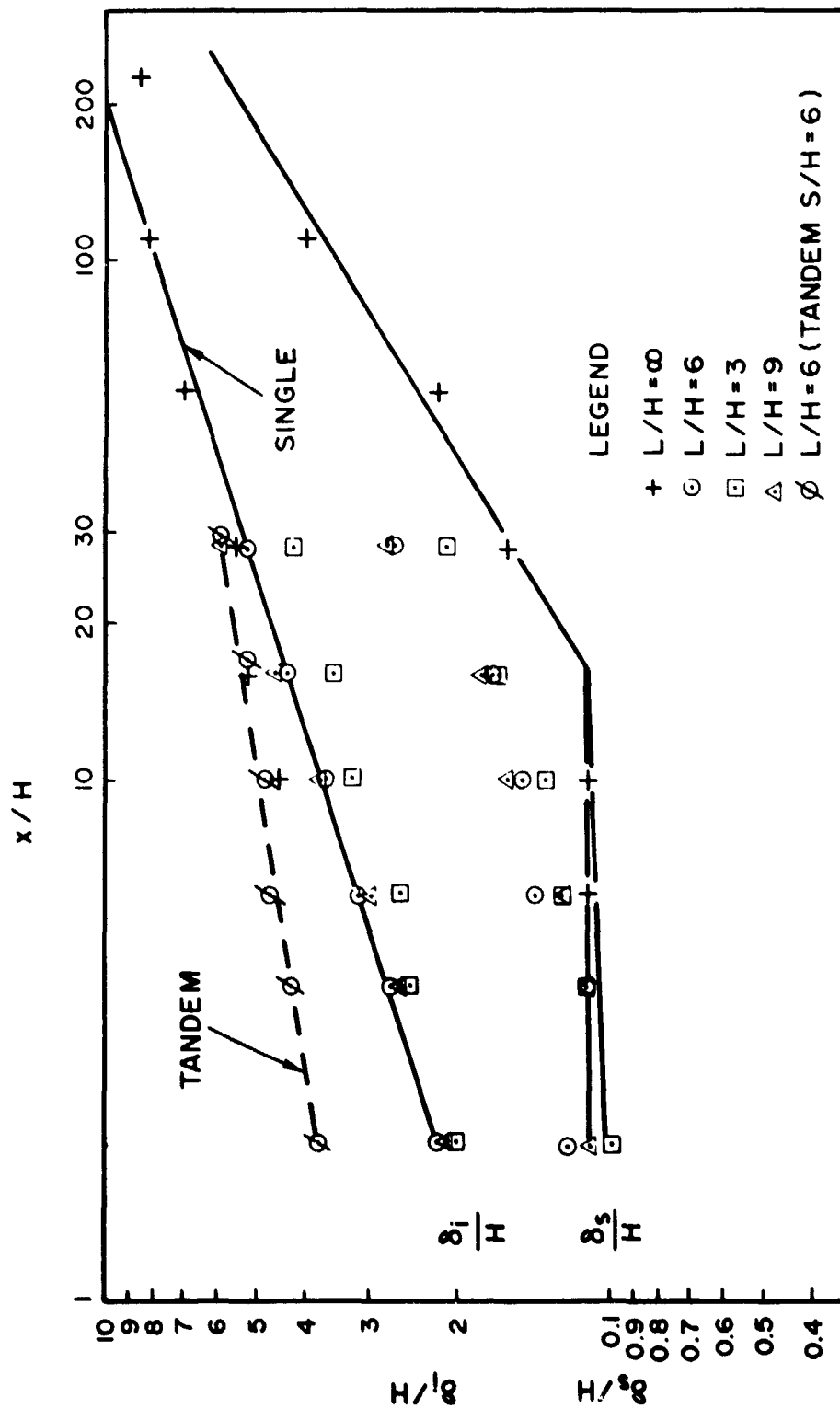
Fig. 47. Boundaries of the Disturbed Region behind Single Buildings

64
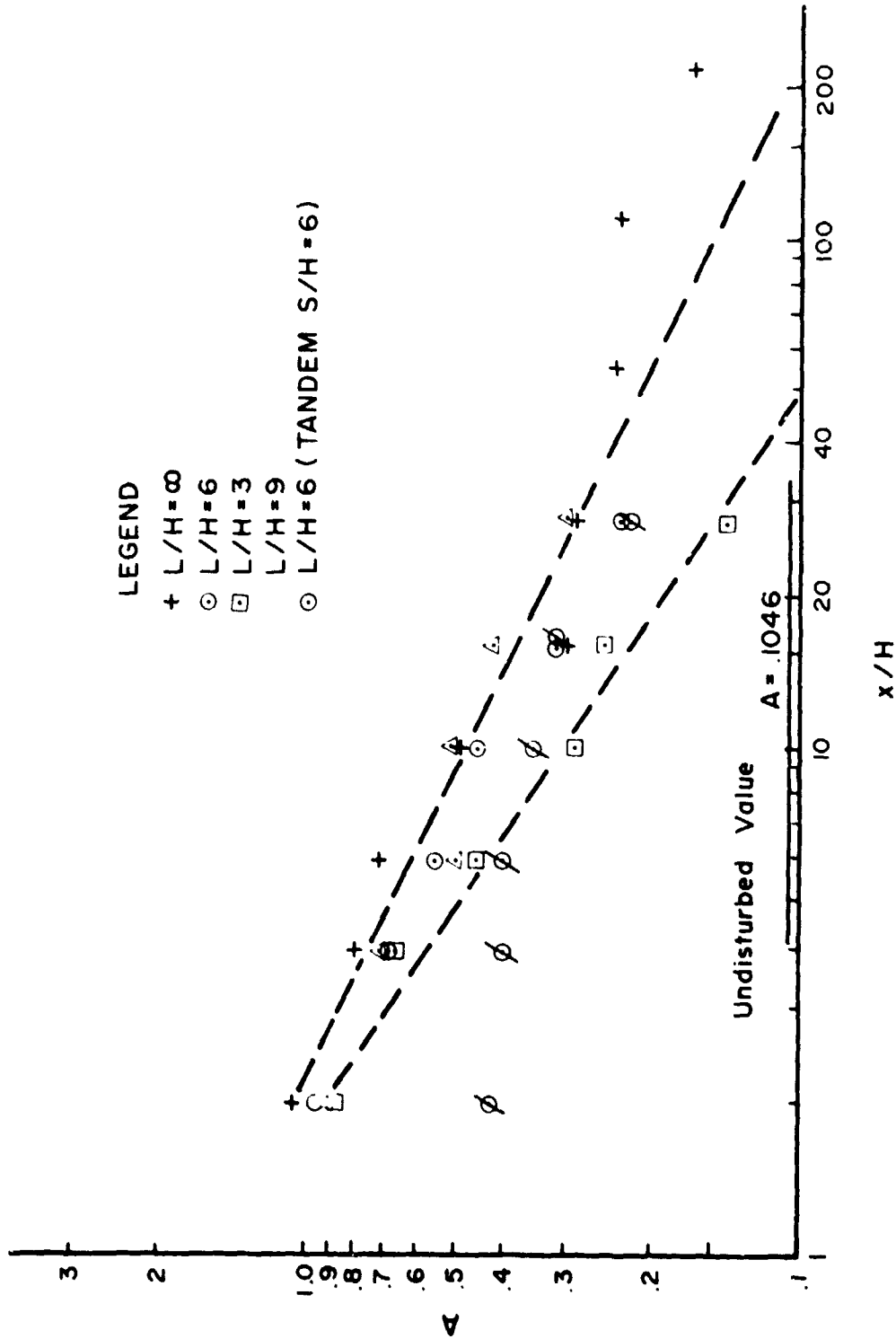
Fig. 48. Slope of the Velocity Profile in the Disturbed Region behind
Single Buildings

Values of the constant A for single buildings are plotted in Fig. 48. A higher value of A means a higher value of dU/dy at a given elevation y. Figure 48 shows that increasing the aspect ratio L/H also increases A. Since the relation between A and skin-friction coefficient is given by

$$A = 2.5 \sqrt{\frac{C_f}{2}} \qquad (4.4)$$

it is evident that C_f increases with L/H also.

The upstream profile corresponds to C_f 0.0035 or A = 0.1046. The disturbed values of A for single buildings lie in the region bounded by the dashed curves of Fig. 48. The upper curve represents roughly the variation of A with x/H when L/H is infinite, and the lower curve represents values of A for L/H = 3. Extrapolation of the data shows that the wake of a building of small aspect ratio decays much faster. The value of x/H at which the curve reaches A = 0.1046 is the length of the disturbed region or wake. Figure 48 is useful in making estimates of wake length, which is the region of potentially hazardous air travel. The height of the region of hazardous flight is determined from Fig. 47, after the length of the region is known from Fig. 48.

The length of the zone of hazardous flight could also be estimated by writing equations for the solid lines of Fig. 47 and solving them simultaneously. The equation for the upper line is given by

$$\frac{\delta_i}{H} = 1.75 \left(\frac{X}{H}\right)^{.3288} \qquad (4.5)$$

and that for the lower boundary is

$$\frac{\delta_s}{H} = 0.192 \left(\frac{x}{H}\right)^{.63} \tag{4.6}$$

Since δ_i/H achieves a value of 10 at $x/H = 200$, and this is the edge of the wind tunnel boundary layer, the extinction of the disturbed region occurs when $\delta_s/H = 10$, viz., about $x/H = 500$. This is somewhat longer than the region obtained by extrapolation of the limited data of Fig. 48. However, the slow decline in the value of A for the building of infinite aspect ratio makes the latter estimate more plausible.

It should be noted that C_f in (4.4) is related to the C_D in (1.2), rather than to the local wall skin friction. The lower part of the profiles, below $y = \delta_s$, have slopes related to the local C_f. This disturbed part of the profile and the corresponding slope A are affected primarily by the force on the model, i.e., by C_D. As seen previously in Fig. 4, C_D decreases as L/H decreases. Thus it is expected that A would decrease with L/H as is depicted in Fig. 48.

The height δ_i of the disturbed region is increased by the tandem arrangement (Patterns 5-7), as is depicted in Fig. 47. The differences in δ_i disappear further downstream, viz., by $x/H = 30$. Values of slope A are lower initially, but differences disappear by $x/H = 16$.

The tandem arrangement of Patterns 5-7 are repeated in Patterns 9-11, which provide two tandem rows spaced laterally by a distance of 6H. Here it is assumed that wake profiles on the building centerlines will be as given for Patterns 5-7 in Figs. 29-34. The wake profiles created along the centerline of the gap between building rows are presented for Patterns 9-11 in Figs. 37-42. Although not an identical

geometry, a comparison with the wide-gap results of Logan and Barber (1980) can be made. The disturbance region is shown in Fig. 49 and may be considered to be included between the dashed curves. Figure 50 shows the variation of A with x/H. Its value is around 0.2 over the entire range, which is almost twice the undisturbed value. The gap data do not show a rapid decay, but it is expected that the decay, indicated by the dashed curve is more appropriate for rows of low aspect-ratio buildings.

Merging of the two dark wedges observed on the photographs of Fig. 14 occured at about x/H = 24 for L/H = 6. This position should correspond with the observed maximum value of A, i.e., to the distance required for the retarding effect behind the obstacle to reach the centerline of the space between the obstacles. The points of Fig. 50 for L/H = 6 show that A maximizes between x/H = 16 and x/H = 28. If the effect spreads laterally a distance of 3H at x/H = 24, then the lateral rate of spread is roughly the same as the vertical rate, as may be inferred from the upper (solid) curve of Fig. 47.

A single building downstream of the gap formed by two laterally spaced buildings was studied and data are presented in Figs. 43-46. The wake profiles for the single building behind the gap (Patterns 12 and 13) were compared with profiles for the single building (Pattern 1). Little effect is noted in values of δ_i and δ_s. However, as significant difference in A occurs at small values of x/H. The small acceleration of fluid which occurs in the gap region results in higher velocity gradients downstream of the building. For Pattern 13, the value of A is increased by 35 percent at x/H = 4 over the value for the building in undisturbed wind. Further comparisons can be made using the numerical data presented in Table A-7 in the Appendix.
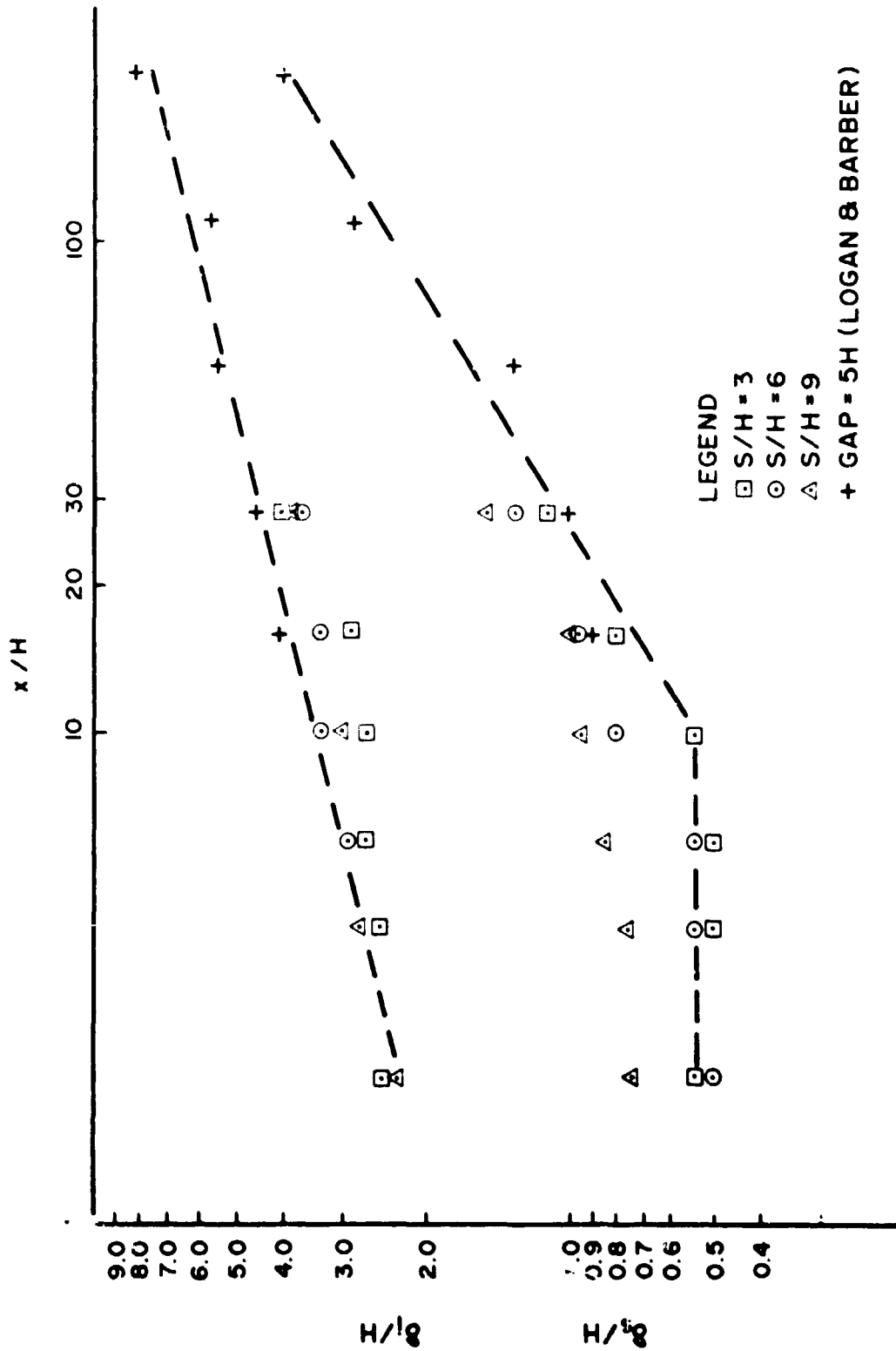
Fig. 49. Disturbed Region on a Line Between Two Rows of Buildings

LEGEND
□ S/H = 3
⊙ S/H = 6
△ S/H = 9
+ GAP = 5H (LOGAN & BARBER)

LEGEND
⊡ S/H = 3
⊙ S/H = 6
△ S/H = 9
+ GAP = 5H (LOGAN & BARBER)

x/H

A

1.0
0.6
0.5
0.4
0.3
0.2
0.1

10   20   30   100   200
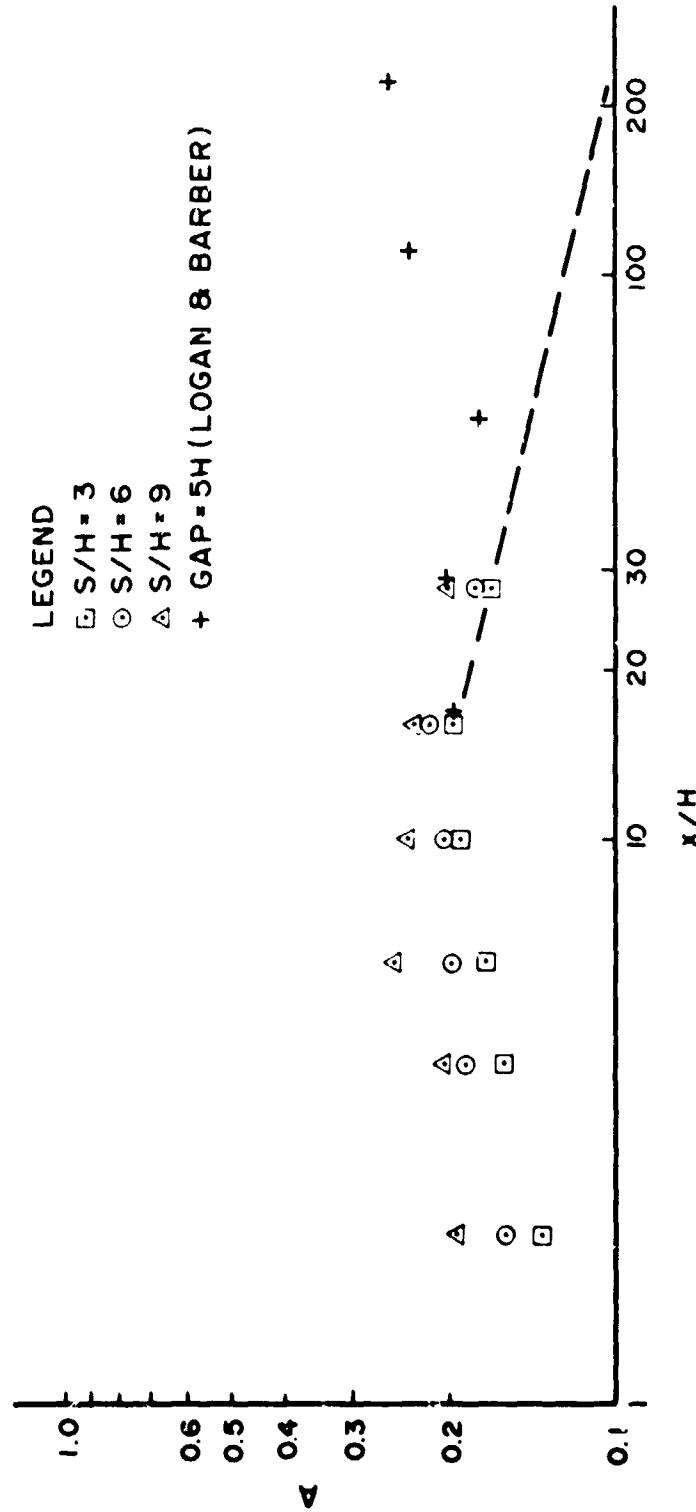
Fig. 59. Slope of the Velocity Profile in the Disturbed Region Between
Two Rows of Buildings

CHAPTER 5

TURBULENCE DISTRIBUTION

Hot-film-probe measurements of u', the rms value of the longitudinal velocity fluctuation, are presented in Figs. 51-76. The fluctuation u' is non-dimensionalized with U^*, the friction velocity of the undisturbed flow.

In these profiles an increase of u' is observed immediately behind the building. The maximum value of u' occurs at elevations of 1-1.5H above the ground at $x/H = 2$. The location of the maximum of u' is denoted by δ_m, and the maximum fluctuation is denoted by u'_m. These locations and magnitudes are presented systematically in Table A-7 of the Appendix.

The extent of the region of increased turbulence may be observed by comparing the wall profiles with the profile for undisturbed flow. This is shown in Fig. 51 to illustrate the clear definition of the region. The upper limit, or merge point, corresponds closely with the position of the upper bend in the velocity profile, i.e., it occurs at or near $y = \delta_i$. The location of the point of maximum turbulence occurs nearer to δ_s, i.e., in the lower part of the zone of high velocity gradient. From (4) it is clear that dU/dy is largest near the bottom of the high-gradient zone, i.e., near $y = \delta_s$, and turbulence production is proportional to dU/dy. The turbulence production also depends on the Reynolds shear stress uv, and this has been shown to maximize in a manner analogous to the turbulence fluction. [See Logan and Chang (1980)]. Prandtl's mixing length theory indicates a dependence of
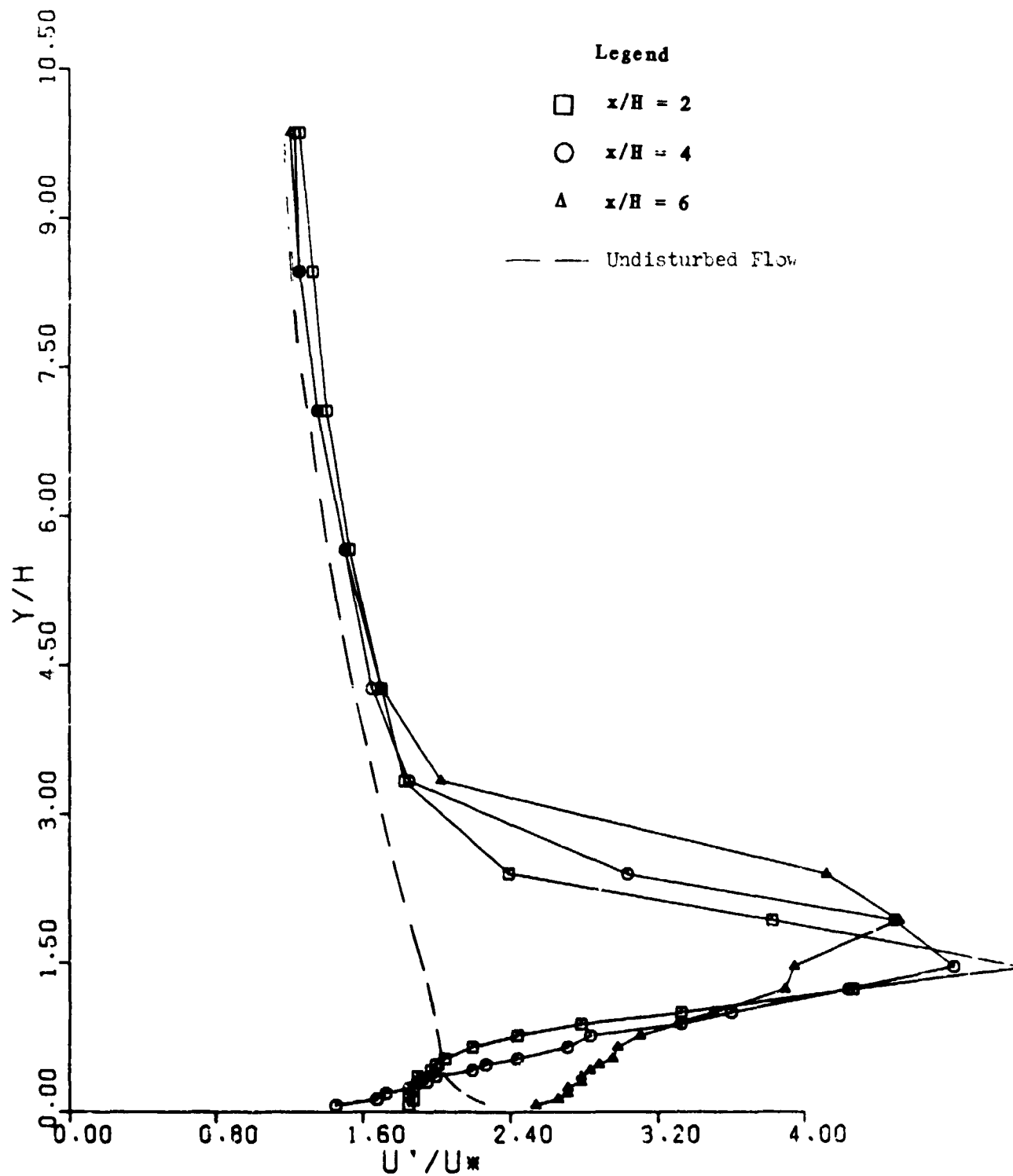
71

Fig. 51. Turbulence Profiles for Pattern No. 1

72

Fig. 52. Turbulence Profiles for Pattern No. 1

Fig. 53. Turbulence Profiles for Pattern No. 2

74
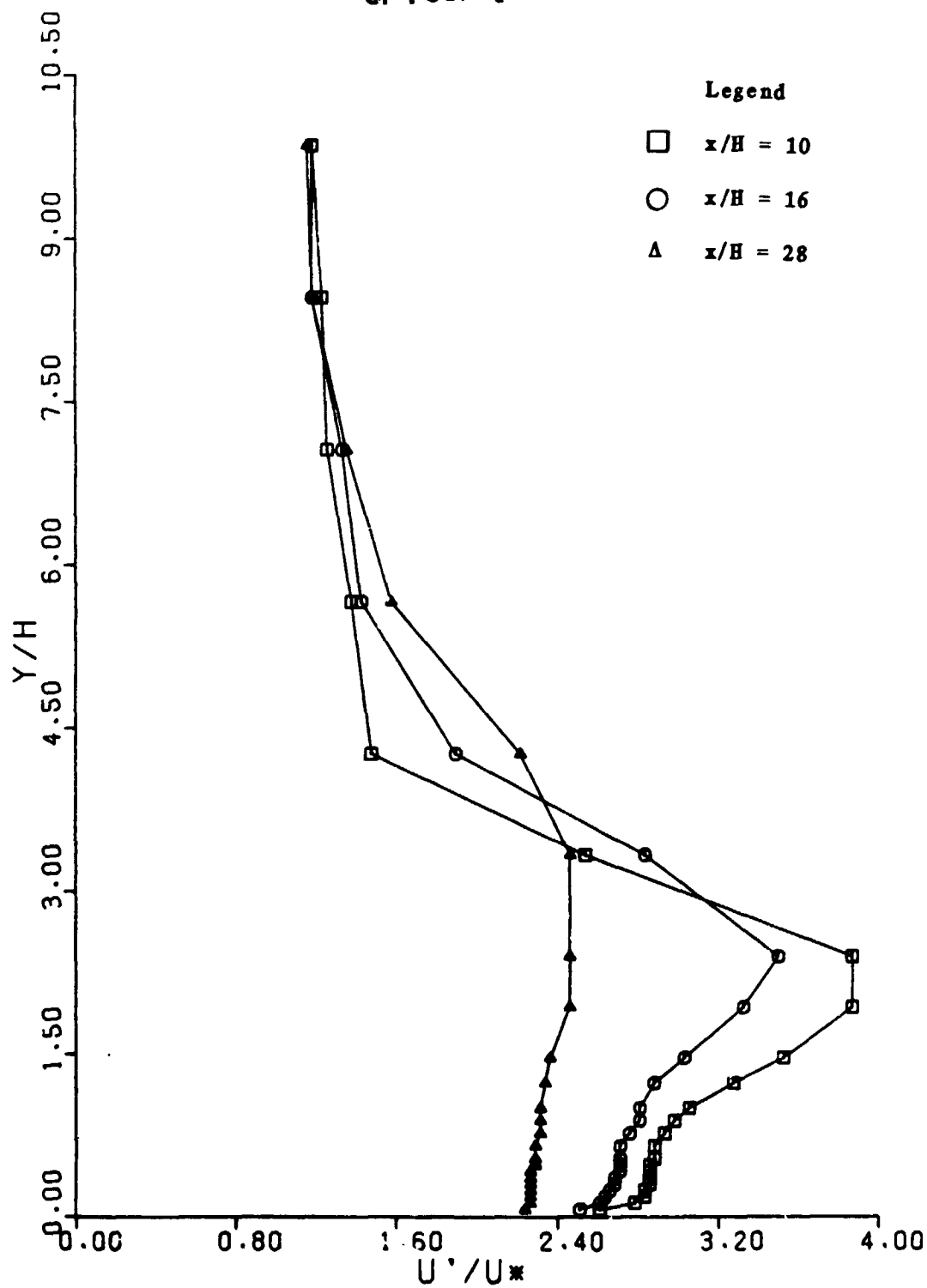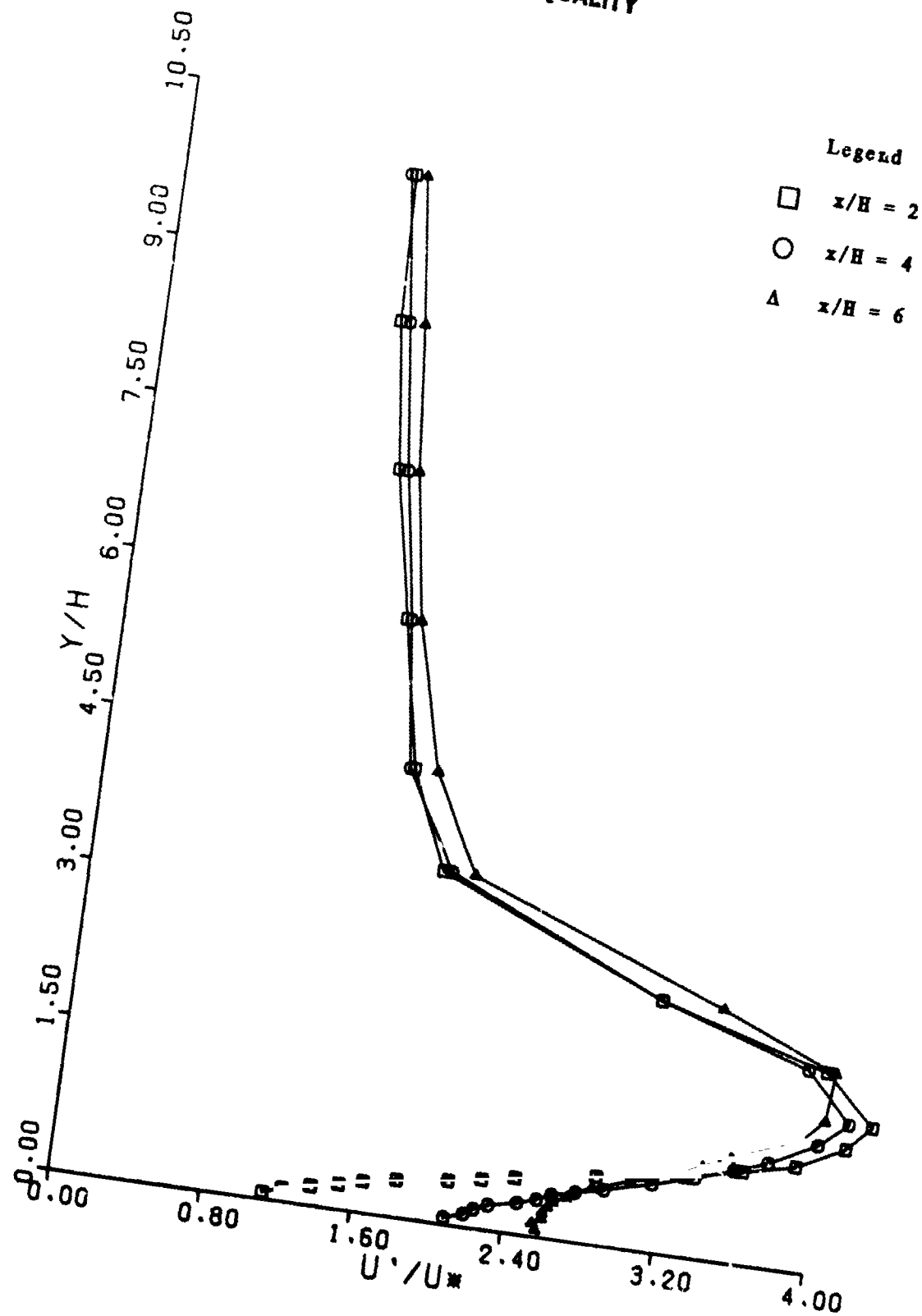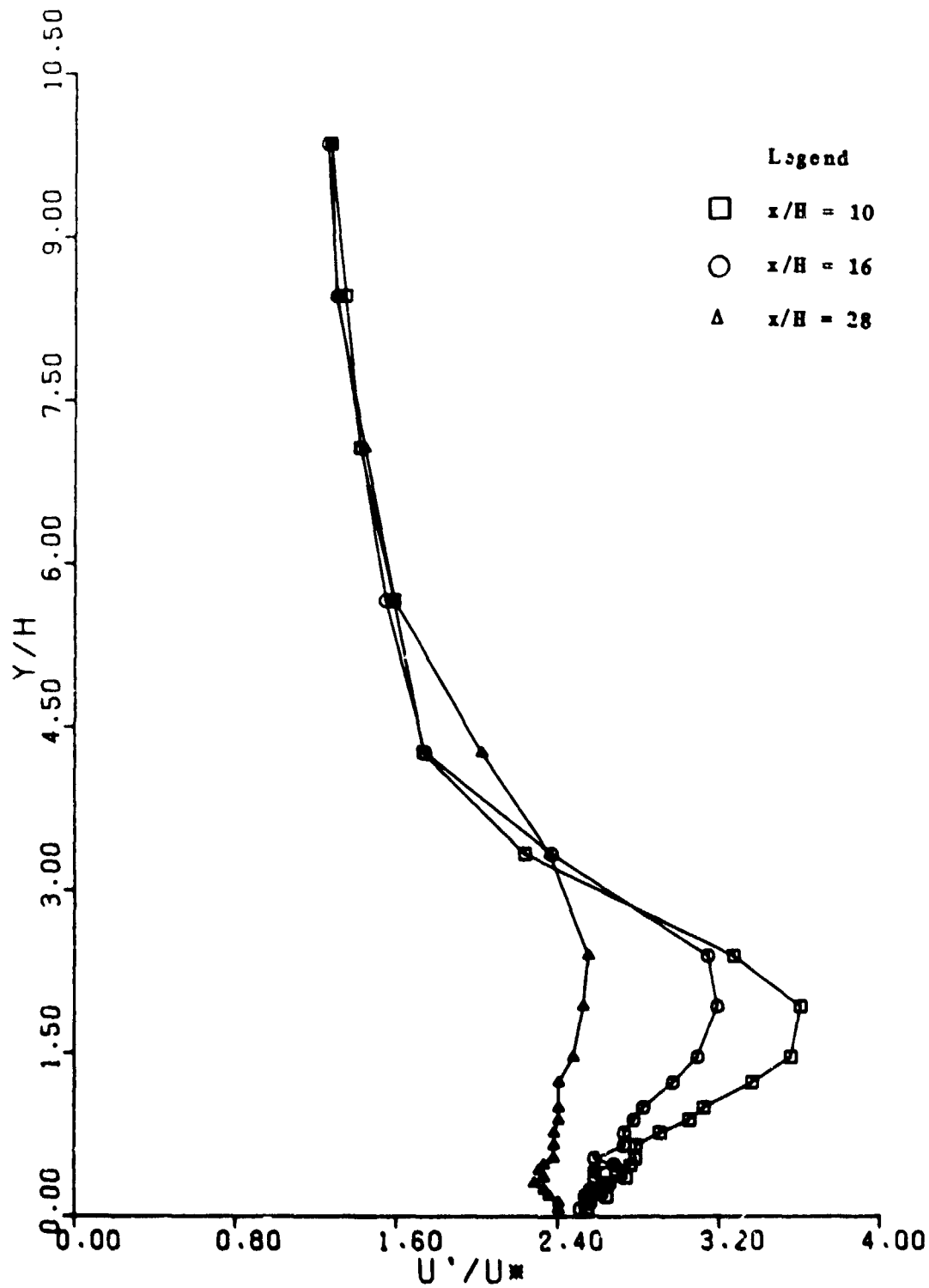
Fig. 54. Turbulence Profiles for Pattern No. 2
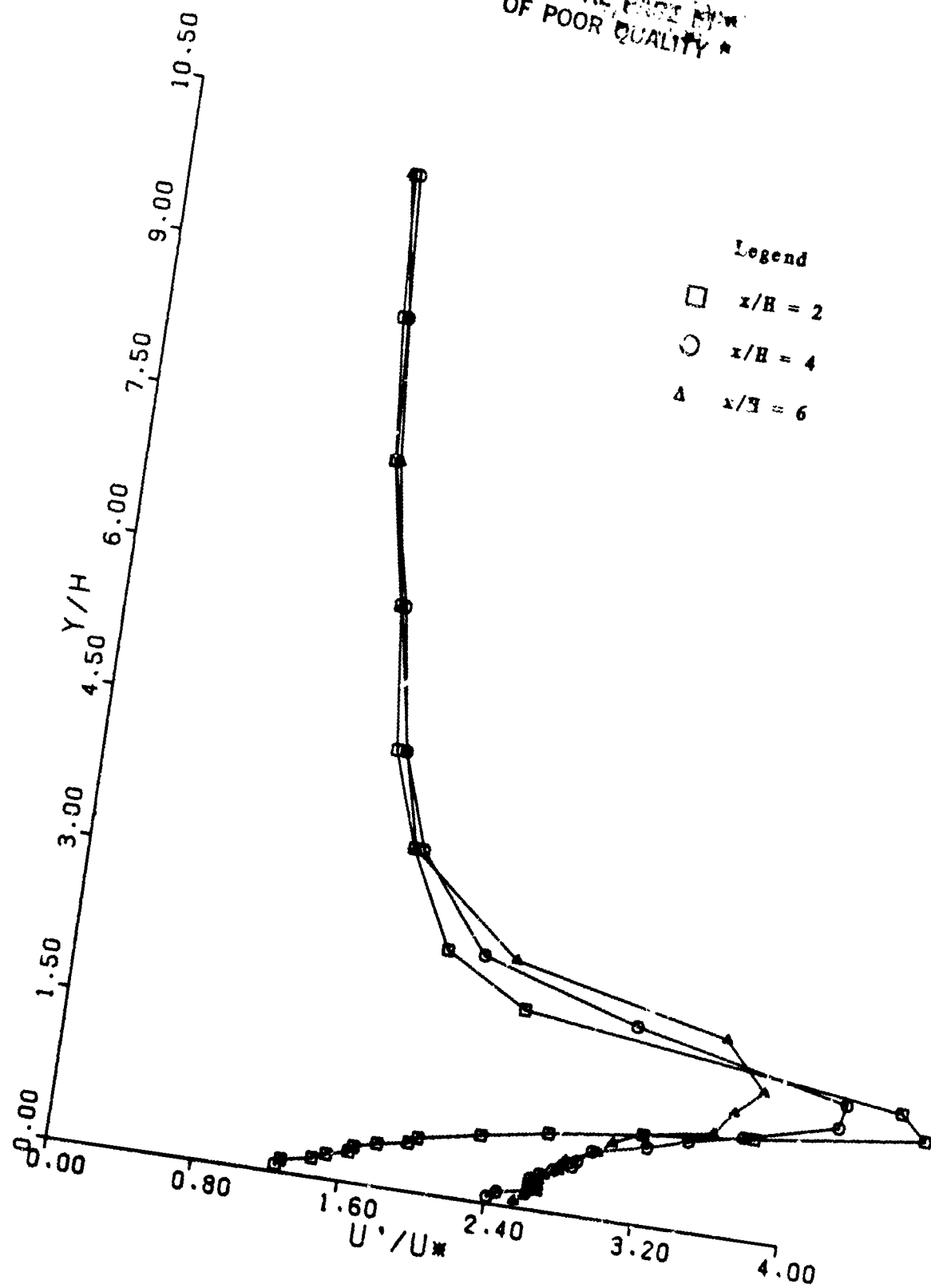
Fig. 55. Turbulence Profiles for Pattern No. 3

Legend

□ x/H = 2

○ x/H = 4

△ x/H = 6

76

Fig. 56. Turbulence Profiles for Pattern No. 3
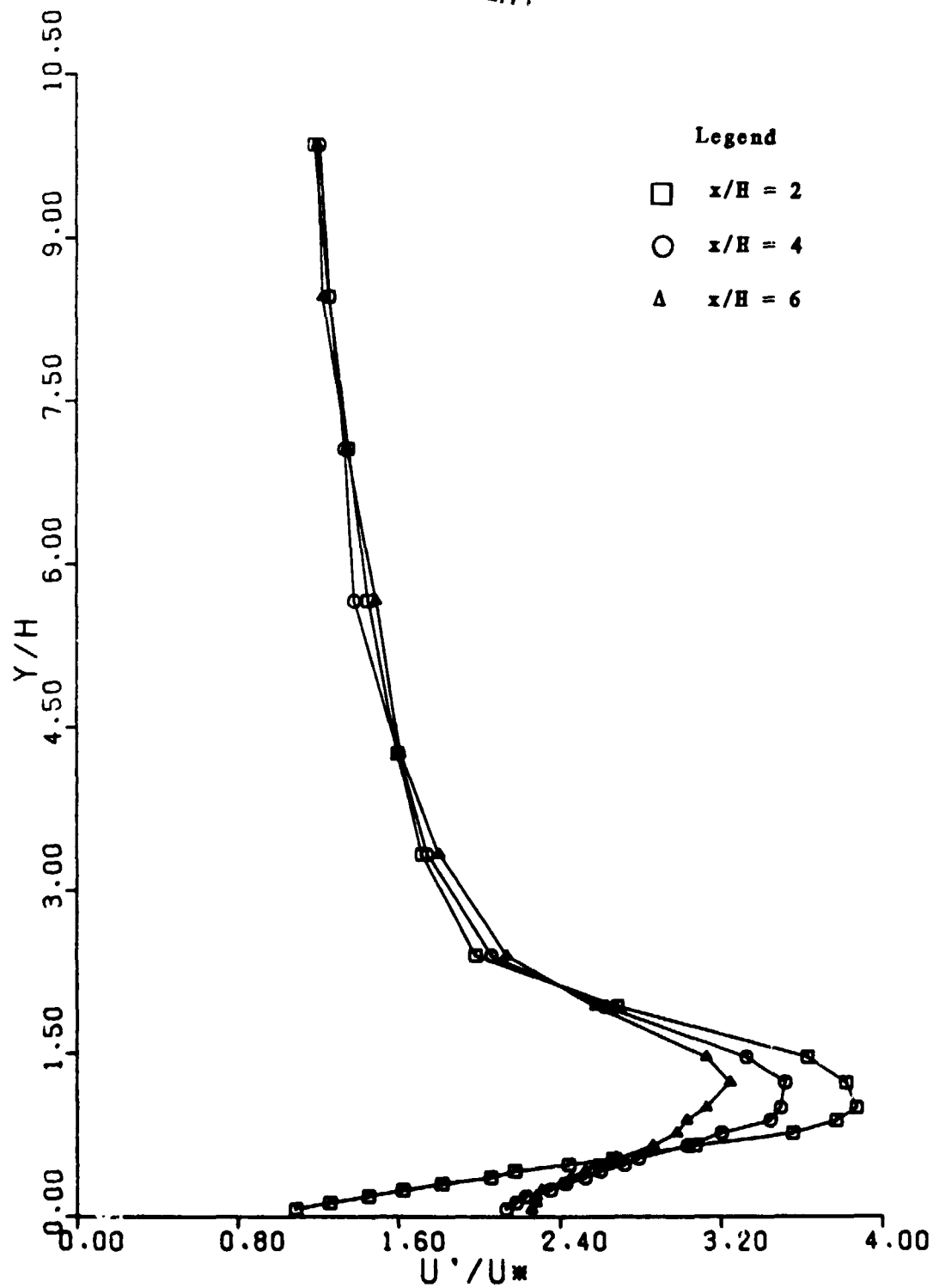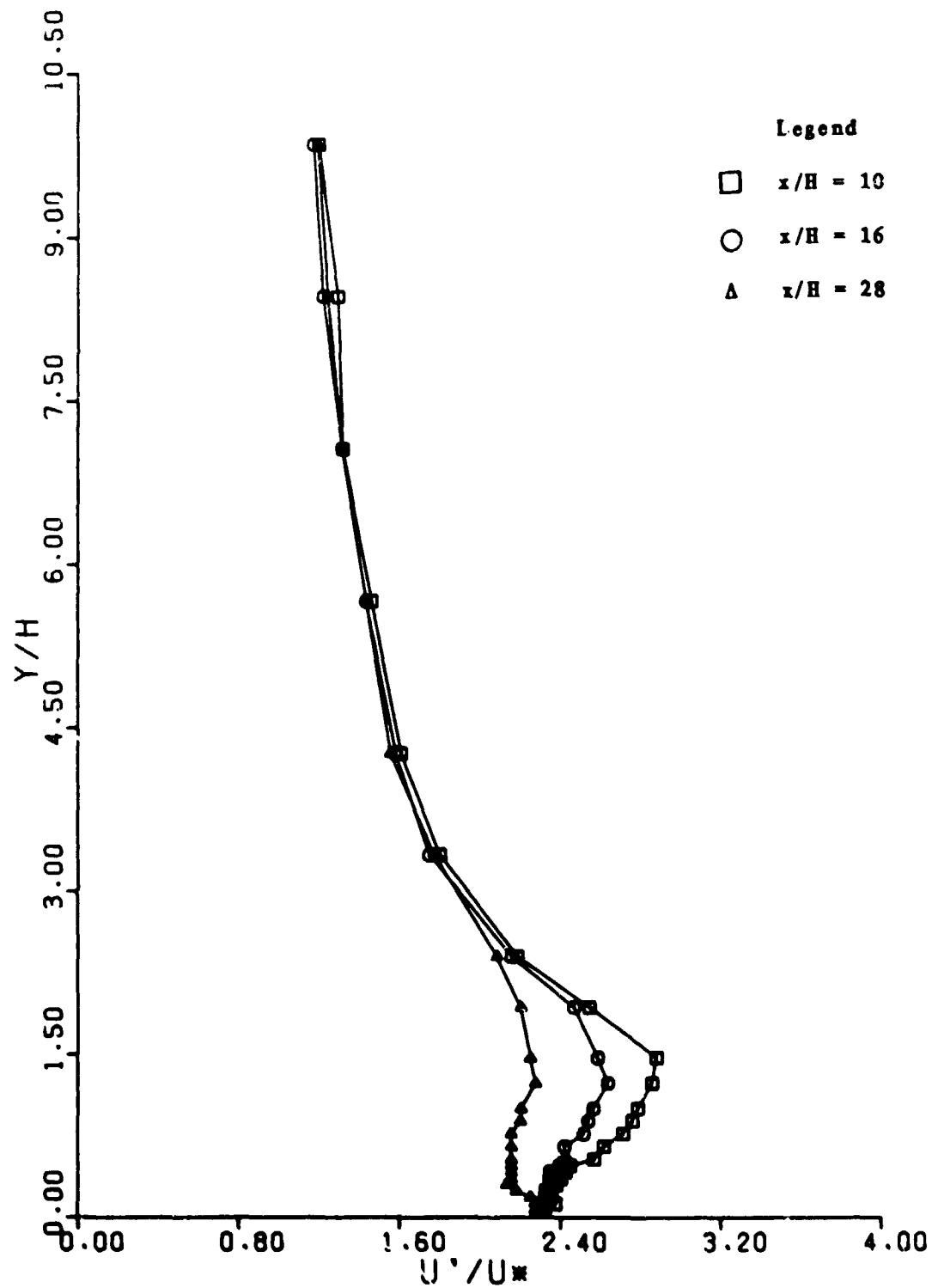
Fig. 57. Turbulence Profiles for Pattern No. 4
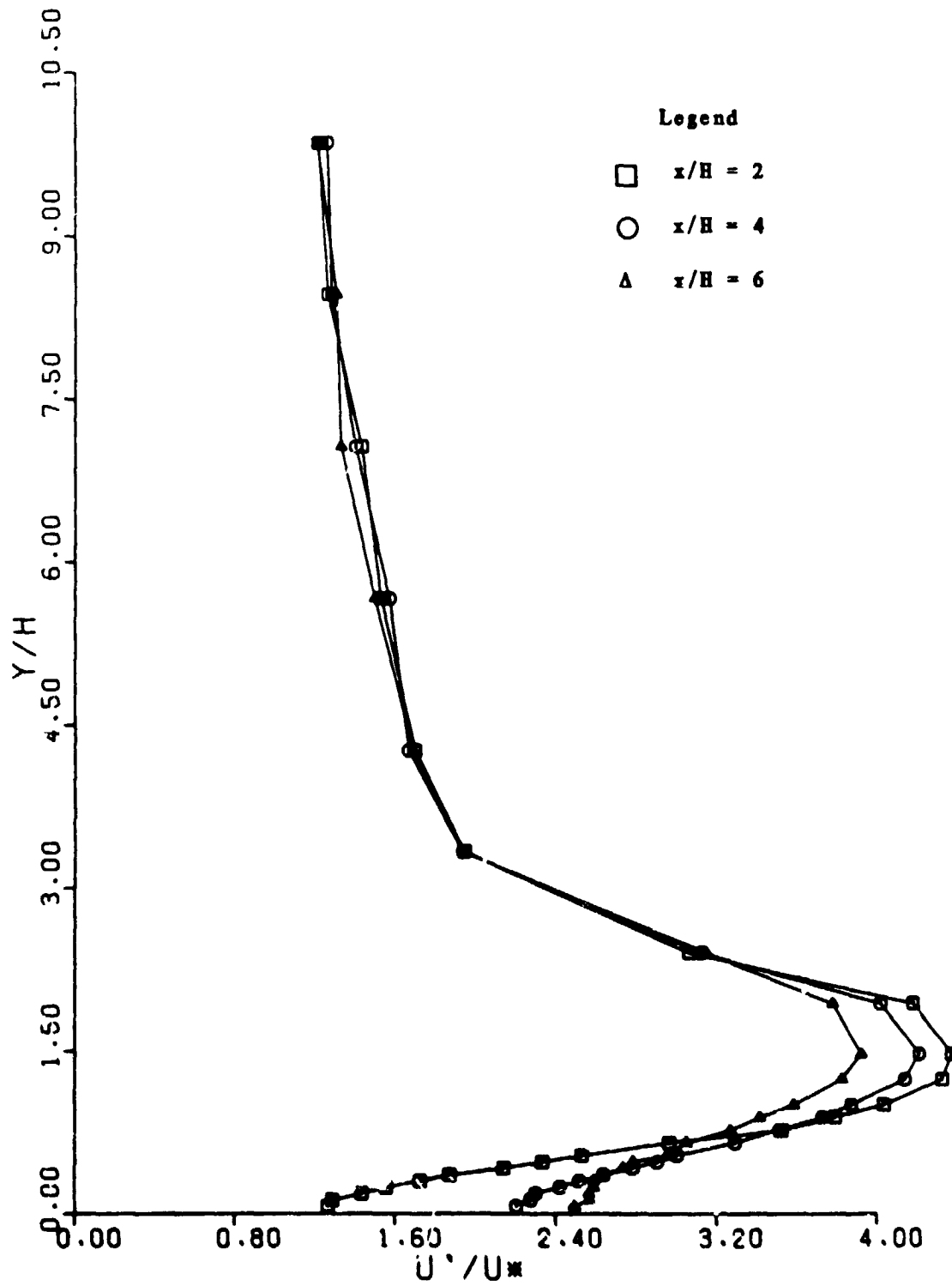
Fig. 58. Turbulence Profiles for Pattern No. 4

Fig. 59. Turbulence Profiles for Pattern No. 5
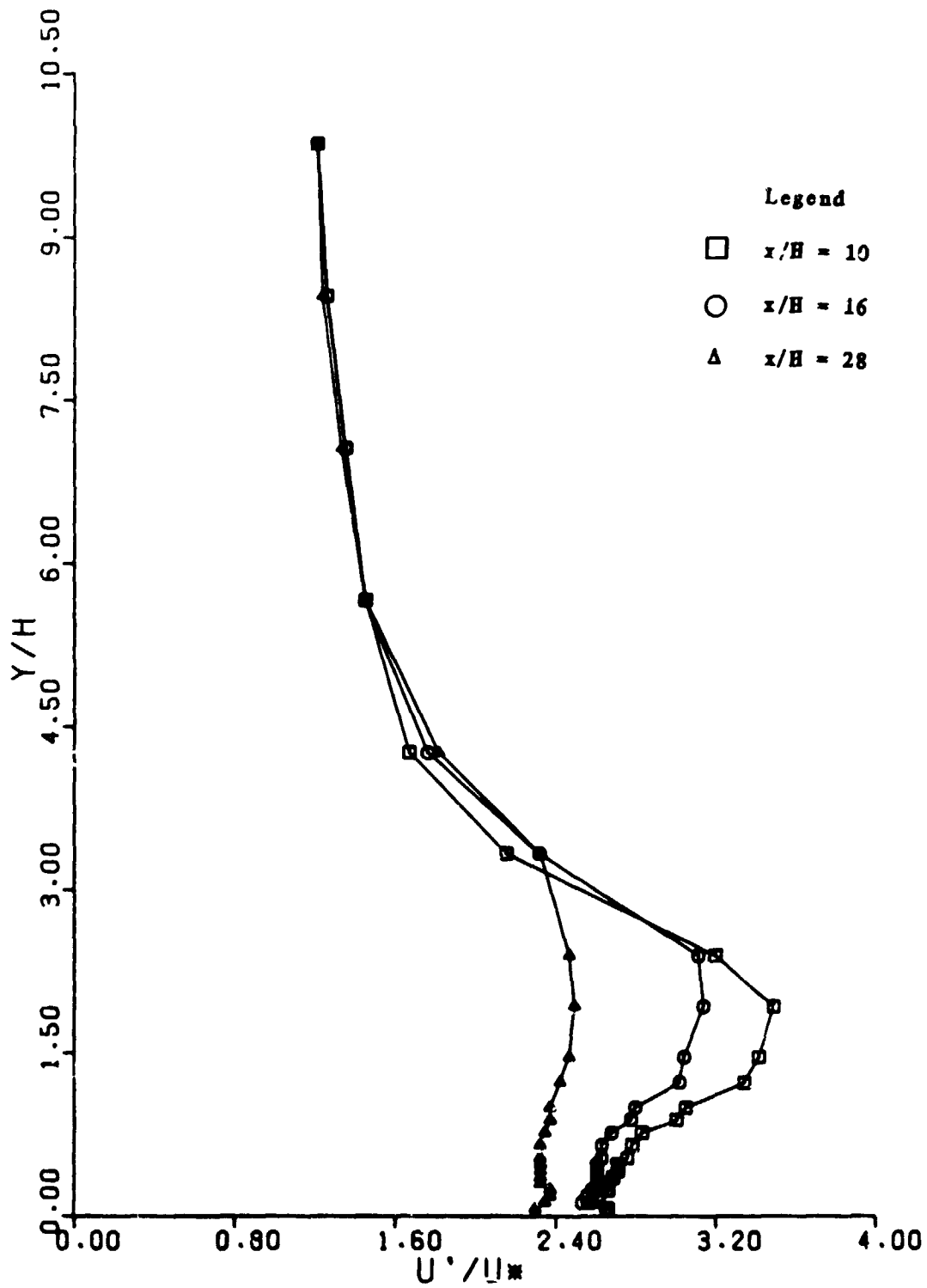
Fig. 60. Turbulence Profiles for Pattern No. 5

Legend

☐   x/H = 2

○   x/H = 4

∧   x/H = 6

Fig. 61. Turbulence Profiles for Pattern No. 6

82

Fig. 62. Turbulence Profiles for Pattern No. 6

Fig. 63. Turbulence Profiles for Pattern No 7

Fig. 64. Turbulence Profiles for Pattern No. 7

85

C-2

Fig. 65. Turbulence Profiles for Pattern No. 8

Fig. 66. Turbulence Profiles for Pattern No. 8

Fig. 67. Turbulence Profiles for Pattern No. 9

Fig. 68. Turbulence Profiles for Pattern No. 9

Fig. 69. Turbulence Profiles for Pattern No. 10

Fig. 70. Turbulence Profiles for Pattern No. 10

Fig. 71. Turbulence Profiles for Pattern No. 11

Fig. 72. Turbulence Profiles for Pattern No. 11

93

Fig. 73. Turbulence Profiles for Pattern No. 12

94

Fig. 74. Turbulence Profiles for Pattern No. 12

Fig. 75. Turbulence Profiles for Pattern No. 13

Fig. 76. Turbulence Profiles for Pattern No. 13

Reynolds shear stress on the square of l(dU/dy), where l is the mixing length.

Turbulence in the region below $y = \delta_s$ is still elevated above the undisturbed value. The region is supplied with 'urbulence energy via gradient diffusion from the higher production zone. Turbulence energy is lost from this region by dissipation in smaller eddie⁻ and by gradient diffusion in the lateral direction, i.e., in the z-direction.

Although the discussion given about fits the wakes directly behind obstacles, it does not suit the development of profiles measured in line with the centerline of the space between two rows of buildings. Profiles for Patterns 9-11 are shown in Figs. 67-72, and they are representative of the second kind of wake. The flow in these regions derives its changed form by adjusting to the highly sheared flow at either side. Momentum is lost to adjacent slower-moving fluid via Reynolds shear stresses associated with lateral variation of mean velocity. Turbulent energy is gained in this region via diffusion from more energetic shear zones and through secondary currents which convect turbulence into this zone near the wall (see Fig. 77). The latter concept of secondary cells was advanced by Rotta (1972) and was based on the shape of isotachs downstream of surface-mounted spheres. The effect of the building on the boundary layer, viz., increased velocity gradient and turbulence, propagates laterally at roughly the same rate as vertically. The effect has been propagated fully to the centerline between the rows of buildings by $16 < x/H < 28$, as seen in Fig. 68 for Pattern 10. Study of surface flow patterns and velocity profiles indicates that the effect maximizes between $x/H = 16$ and $x/H = 28$. Beyond this station, turbulence and slope A decline. Because the effect is propagated from the
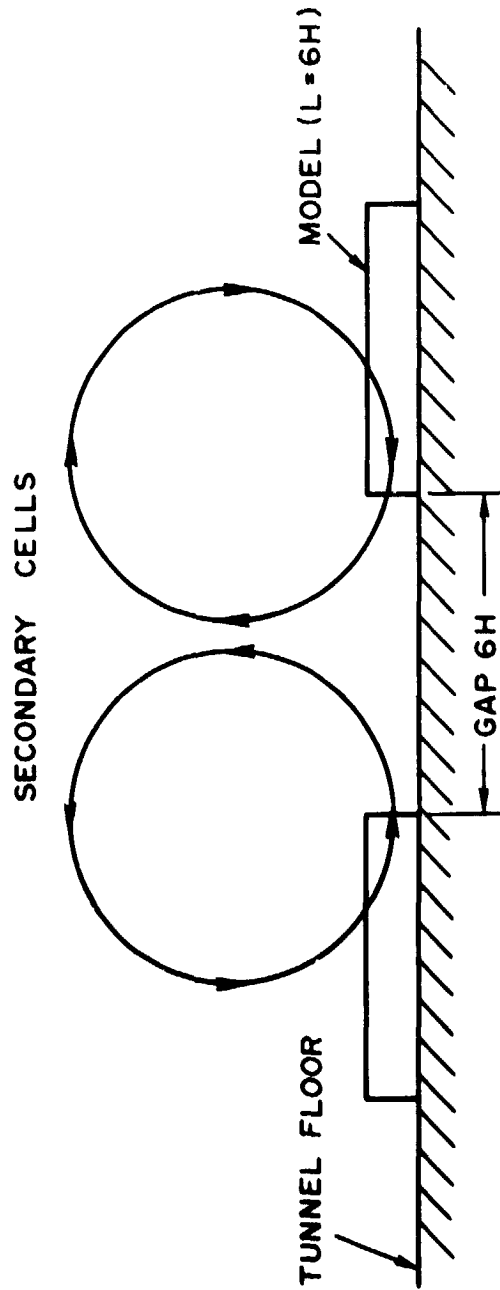
Fig. 77. Secondary Cells behind Rows of Surface-mounted Obstacles

first element of the two in tandem, forming of the profiles begins earlier in Fig. 71 for Pattern 11, than for Pattern 9 and 10.

One inference that can be made from these data is that the lateral spread rate is roughly the same as the vertical rate of spread. This is in agreement with predictions made in an earlier section from velocity profile changes and from surface flow visualization. This approximate method may be used to predict the lateral extent of the wake and to make estimates of the slope A and maximum values of u' on the sides of the model. The method should be checked in future research.

CHAPTER 6

COMPARISON OF WAKES

Some important data for each pattern used in the present study are compared in Table II. The first three columns of the table refer to the last station, i.e., $x/H = 28$. For this station the first column contains the height of the shear layer in building heights. The second column lists the height of the layer of maximum turbulence level at $x/H = 28$. The third column presents the increase in turbulence level above the original or upstream value u'_o at the elevation δ_m/H where u' has its maximum value. This turbulence excess $u'_m - u'_o$ is non-dimensionalized with the upstream or undisturbed friction velocity U^*. The fourth column lists values of non-dimensional velocity gradient in the shear layer formed in the wake between $y = \delta_i$ and $y = \delta_s$. The gradient shown is the maximum at the arbitrary height $y = 3H$. In this chapter values in Table II will be used to compare the wakes produced by the 13 patterns of buildings. From the standpoint of flight safety, patterns having the smallest values of quantities in Table II are preferred.

Patterns 1, 3 and 8 are the single, block-type structure with its length normal to the flow. From Table II it is seen that increasing L/H increases the thickness δ_i of the shear layer. The magnitude and height of the high turbulence zone also are found to increase with aspect ratio. The magnitude of the velocity gradient increases when L/H is increased from 3 to 6 but does not change significantly when L/H changes from 6 to 9. A smaller aspect ratio is clearly desirable.

TABLE II

COMPARISON OF WAKES

| PATTERN | x/H = 28 | | | max. at y/H = 3 |
No.	δ_i/H	δ_m/H	$(u'_m-u'_o)/U*$	$d(U/u')/d(y/H)$
1	5.6	2.7	.7	.18
2	4.8	2.6	.6	.17
3	4.2	2.4	.4	.10
4	3.5	2.3	.5	.07
5	4.8	2.4	.7	.14
6	5.8	3.3	.8	.14
7	5.5	3.3	.8	.14
8	5.9	3.3	1.3	.17
9	4.0	1.9	.7	.06
10	3.6	1.9	.6	.07
11	3.8	1.9	.7	.08
12	6.0	3.3	1.2	.19
13	5.7	3.3	1.1	.20

Tandem arrangement of two buildings of equal length was employed in patterns 2, 4, 5, 6 and 7. Pattern 4 can be compared with Pattern 3, since L = 3H in both cases. A small improvement is observed for the closely-spaced, low-aspect-ratio buildings. Patterns 5, 6 and 7 can be compared with pattern 1, as all buildings have L/H = 6. The closely spaced, tandem arrangement, pattern 5, shows an improvement in all categories, while wider spacing does not improve the wake in an overall sense. Thus the tandem arrangement with S/H = 3 is preferred over the single building.

No significant differences are observed in the wake of the gap between the rows of the 4-building arrays, patterns 9, 10 and 11. Based on data from the tandem patterns, it appears that the pattern 9 is to be preferred. One point that should be studied in the future is the magnitude of secondary air currents set up by the rows of buildings. In future investigations three or more buildings could be included in each row, and the velocity components, U, V and W, measured.

The arrangement of a single building behind the gap formed by two laterally spaced buildings appears to be a very bad design. The wake of the single building in patterns 12 and 13 can be compared with that of the isolated building in pattern 1. The gap appears to affect the wake adversely for both longitudinal spacings. Further study could prove that tandem arrangement with short longitudinal spacing would be superior in this case as well, i.e., in the case of a 3- or 4-building array of buildings of unequal lengths.

An extension of the present research, which seems worthwhile, would be an attempt to optimize spacing in the tandem arrangement for various aspect ratios. The data of Table II show that such an optimum may exist. The effect two or more buildings of different heights in a tandem array should also be addressed.

REFERENCES

Cermak, J.E., ''Applications of Fluid Mechanics to Wind Engineering - a Freeman Scholar Lecture'', J. Fluids Eng., Vol. 97, 1975, pp. 9-38.

Fichtl, G.H., Camp, D.W. and Frost W., ''Sources of Low-level Wind Shear Around Airports'', J. Aircraft, Vol. 14, pp. 5-14, 1977.

Frost, W., Fichtl, G., Connell, J.R. and Hutto, M.L., ''Mean Horizontal Wind Profiles Measured in the Atmospheric Boundary Layer about a Simulated Block Building'', Boundary Layers Meteorology, Vol. 11, pp. 135-145, 1977.

Holdredge, E.S. and Reed, B.H., ''Wind Tunnel Studies of Pressure and Velocity Distribution'', Texas Engineering Experiment Station Report, Contract DA-18-064-404-CML-189, College Station, Texas, 1956.

Hunt, J.C.R., ''The Effect of Single Buildings and Structures'', Phil. Trans. Roy. Soc. Lond. A 269, pp. 457-467, 1971.

Joubert, P.N., Perry, A.E. and Stevens, L.K., ''Drag of a Bluff Body Immersed in a Rough-wall Boundary Layer'', Proceedings of the Third International Conference on Wind Effects on Buildings and Structures, Saikon, Tokyo, 1971, pp. 179-188.

Logan, E. and Barber, D.S., ''Effect of Lateral Spacing on Wake Characteristics of Buildings'', NASA CR-3337, Marshall Space Flight Center, 1980.

Logan, E. and Camp, D.W., ''Preliminary Comparison of Model and Prototype Wakes'', AIAA Paper 78-254, 1978.

Logan, E. and Chang, J., ''Wake Characteristics of Buildings in Disturbed Boundary Layers'', NASA CR-3284, Marshall Space Flight Center, 1980.

Logan, E. and Lin, S.H., ''Wind Tunnel Measurements of Three-dimensional Wakes of Buildings'', NASA CR-3565, Marshall Space Flight Center, 1982.

McDonald, H. and Kreskovsky, J.P., ''Effect of Free Stream Turbulence on the Turbulent Boundary Layer'', Int. J. Heat Mass Transfer, Vol. 17, 1974, pp. 705-716.

Penwarden, A.D. and Wise, A.F.E., ''Wind Environment Around Buildings'', Building Research Establishment Report, 1975.

Pletcher, R.H. and McManus, H.N., ''Secondary Flow in the Entrance Section of a Straight Rectangular Duct'', in S. Ostrach, Ed., Developments in Mechanics, Vol. 2, 1965, pp. 269-291.

Rotta, J.C., *Turbulente Stromungen*, Teubner, Stuttgart, 1972.

Wieghardt, K., ''Erhohung des Turbulenten Reibungswiderstandes durch Oberflachenstorungen'', *Forschung fur Schiffbau und Schiffmaschinen*, No. 2, pp. 65-81.

A.F.E. Wise, D.E. Sexton and M.S.T. Lillywhite, ''Studies of Air Flow round Buildings'', *Architects Journal*, May 1965, pp. 1185-1190.

Woo, H.G.C., Peterka, J.A. and Cermak, J.E., ''Wind-tunnel Measurements in the Wakes of Structures'', NASA CR-2806, Marshall Space Flight Center, 1977.

APPENDIX

TABLE A-1

Pressure-probe Measurements of U(m/s) for Pattern No. 1 (Table I)

z/H	y/H	x/H 2	4	6	10	16	28
0	1	3.505	3.656	3.895	4.368	4.793	5.211
	2	5.617	5.567	5.108	4.839	5.026	5.388
	3	5.872	5.780	5.782	5.620	5.488	5.589
	4	5.993	5.967	6.000	5.937	5.877	5.783
	5	5.998	6.089	6.031	6.001	6.061	6.092
	6	6.091	6.207	6.151	6.122	6.122	6.182
	8	6.299	6.353	6.357	6.270	6.270	6.299
	10	6.439	6.414	6.414	6.386	6.472	6.499
-2.5	1	4.642	4.946	5.170	5.255	5.226	5.155
	2	5.729	5.576	5.584	5.577	5.513	5.610
	3	5.884	6.067	5.819	5.811	5.747	5.748
	4	6.008	6.036	6.005	5.970	5.909	5.970
	5	6.128	6.127	6.067	6.093	6.002	6.122
	6	6.247	6.247	6.186	6.182	6.124	6.213
	8	6.363	6.391	6.332	6.389	6.361	6.360
	10	6.478	6.534	6.504	6.504	6.504	6.531
-4.5	1	5.466	5.388	5.284	5.184	5.255	5.293
	2	5.817	5.757	5.693	5.692	5.694	5.728
	3	6.008	6.007	5.885	5.917	5.916	5.949
	4	6.069	6.068	6.040	6.100	6.040	5.980
	5	6.190	6.159	6.161	6.161	6.190	6.161
	6	6.307	6.307	6.220	6.249	6.278	6.249
	8	6.423	6.479	6.366	6.423	6.479	6.423
	10	6.536	6.563	6.535	6.508	6.507	6.564
-6.5	1	5.629	5.594	5.526	5.527	5.525	5.973
	2	5.978	5.944	5.944	5.946	5.943	5.974
	3	6.219	6.189	6.189	6.160	6.126	6.214
	4	6.277	6.307	6.278	6.278	6.332	6.364
	5	6.365	6.422	6.335	6.393	6.421	6.450
	6	6.479	6.479	6.479	6.479	6.450	6.506
	8	6.592	6.592	6.592	6.564	6.590	6.618
	10	6.675	6.647	6.647	6.675	6.673	6.701

TABLE A-2

Pressure-probe Measurements* of -V(m/s) for Pattern No. 1 (Table I)

		x/H					
z/H	y/H	2	4	6	10	16	28
0	1	1.172	1.007	.967	.766	.580	.374
	2	.248	.287	.377	.509	.493	.341
	3	.215	.262	.286	.327	.348	.312
	4	.237	.242	.257	.303	.273	.285
	5	.238	.227	.253	.238	.267	.227
	6	.226	.231	.237	.223	.223	.216
	8	.184	.195	.195	.187	.205	.202
	10	.168	.171	.171	.174	.130	.144
-2.5	1	.347	.354	.364	.449	.489	.571
	2	.177	.273	.272	.391	.381	.386
	3	.254	.267	.300	.338	.346	.328
	4	.257	.290	.294	.335	.325	.335
	5	.260	.278	.267	.336	.312	.314
	6	.245	.245	.270	.288	.277	.266
	8	.230	.244	.269	.261	.265	.212
	10	.199	.210	.230	.230	.247	.175
-4.5	1	.325	.321	.357	.352	.363	.336
	2	.205	.232	.240	.260	.279	.256
	3	.220	.182	.235	.215	.231	.209
	4	.212	.231	.179	.190	.198	.186
	5	.180	.202	.183	.165	.198	.183
	6	.184	.184	.159	.191	.170	.173
	8	.154	.147	.125	.136	.147	.136
	10	.141	.155	.106	.110	.161	.103
-6.5	1	.288	.293	.322	.302	.382	.279
	2	.205	.246	.227	.246	.265	.261
	3	.159	.180	.198	.183	.223	.230
	4	.199	.149	.152	.152	.198	.195
	5	.177	.154	.163	.139	.171	.150
	6	.147	.147	.130	.130	.168	.179
	8	.135	.135	.135	.138	.152	.149
	10	.109	.129	.112	.109	.143	.124

*All values in this table are of -V; thus all values of V are negative, i.e., directed downward.

TABLE A-3

Pressure-probe Measurements of W(m/s) for Pattern No. 1 (Table I)

		x/H					
z/H	y/H	2	4	6	10	16	28
o	1	0	0	-.068	-.076	-.084	-.182
	2	-.294	-.187	0	-.084	0	0
	3	-.308	-.202	-.101	-.098	0	0
	4	-.314	-.208	0	0	0	0
	5	-.209	-.213	0	0	0	0
	6	-.106	-.217	0	0	0	0
	8	-.110	-.222	0	0	0	0
	10	-.225	-.112	0	0	0	0
-2.5	1	.986	.783	.726	.552	.457	.360
	2	.100	.307	.390	.390	.325	.392
	3	.103	.106	.101	.304	.301	.301
	4	0	.105	.105	.208	.206	.299
	5	0	0	.106	.106	.210	.213
	6	0	0	.108	.216	.214	.217
	8	0	0	.111	.111	.111	.222
	10	0	0	.113	.113	.113	.228
-4.5	1	.574	.282	.277	.181	.092	0
	2	.305	.201	.199	.199	.099	0
	3	.105	.210	.103	.103	.103	0
	4	.106	.106	.105	.106	0	0
	5	0	.107	0	0	0	0
	6	0	0	0	0	0	0
	8	0	0	0	0	0	0
	10	0	0	-.114	0	0	0
-6.5	1	.098	.195	.193	.193	.096	.208
	2	.104	.207	.207	.104	.207	.208
	3	.108	.108	.108	.108	.214	.219
	4	0	.110	.110	.110	.221	.111
	5	0	.112	.111	.111	.112	.112
	6	0	0	.113	.113	.112	.114
	8	0	0	0	0	.115	.115
	10	0	0	0	0	.116	.117

TABLE A-4

Pressure-probe Measurements of U(m/s) for Pattern No. 6 (Table I)

x/H

z/H	y/H	2	4	6	10	16	28
0	1	3.891	3.892	4.137	4.451	4.830	5.094
	2	4.765	4.682	4.680	4.761	5.021	5.278
	3	5.595	5.392	5.425	5.318	5.386	5.419
	4	5.943	5.911	5.849	5.815	5.751	5.719
	5	6.124	ɩ.065	6.032	6.032	6.003	5.942
	6	6.212	6.213	6.183	6.124	6.125	6.154
	8	6.331	6.360	6.331	6.330	6.273	6.330
	10	6.531	6.503	6.532	6.503	6.503	6.474
-2.5	1	4.685	4.676	4.904	4.979	5.056	5.142
	2	5.273	5.206	5.214	5.279	5.350	5.388
	3	5.753	5.624	5.556	5.553	5.587	5.584
	4	5.877	5.846	5.814	5.814	5.812	5.749
	5	6.000	5.940	6.000	5.969	5.969	5.938
	6	6.060	6.061	6.031	6.031	6.061	6.090
	8	6.269	6.269	6.239	6.211	6.270	6.269
	10	6.410	6.413	6.415	6.386	6.416	6.412
-4.5	1	5.289	5.269	5.150	5.367	5.404	5.280
	2	5.775	5.742	5.782	5.800	5.800	5.743
	3	5.979	5.907	5.937	5.997	6.026	5.967
	4	6.099	6.098	6.097	6.116	6.118	6.059
	5	6.195	6.216	6.216	6.216	6.244	6.177
	6	6.341	6.309	6.311	6.310	6.302	6.295
	8	6.431	6.459	6.425	6.424	6.418	6.442
	10	6.543	6.543	6.594	6.621	6.594	6.555
-6.5	1	5.543	5.510	5.408	5.386	5.335	5.352
	2	5.895	5.864	5.872	5.812	5.812	5.745
	3	6.085	6.055	6.086	6.029	5.999	5.967
	4	6.204	6.115	6.204	6.179	6.179	6.179
	5	6.350	6.350	6.325	6.268	6.239	6.238
	6	6.407	6.407	6.353	6.355	6.326	6.355
	8	6.522	6.522	6.467	6.469	6.441	6.469
	10	6.606	6.606	6.579	6.553	6.553	6.553

TABLE A-5

Pressure-probe Measurements* of −V(m/s) for Pattern No. 6 (Table I)

		x/H					
z/H	y/H	2	4	6	10	16	28
0	1	.963	1.014	.864	.765	.593	.531
	2	.543	.595	.616	.585	.572	.485
	3	.332	.377	.398	.442	.447	.426
	4	.340	.356	.353	.376	.389	.387
	5	.332	.323	.345	.345	.346	.358
	6	.336	.336	.324	.332	.332	.330
	8	.321	.313	.285	.304	.293	.304
	10	.274	.295	.239	.264	.249	.268
−2.5	1	.327	.440	.456	.500	.511	.429
	2	.293	.346	.367	.377	.3r	.383
	3	.290	.307	.317	.357	.377	.372
	4	.311	.315	.319	.339	.357	.367
	5	.312	.302	.331	.335	.316	.339
	6	.322	.304	.308	.308	.322	.336
	8	.276	.276	.298	.284	.276	.294
	10	.275	.275	.240	.244	.240	.292
−4.5	1	.487	.468	.617	.586	.576	.421
	2	.374	.398	.413	.467	.467	.347
	3	.348	.394	.407	.417	.430	.316
	4	.349	.367	.385	.416	.398	.285
	5	.337	.368	.368	.368	.381	.306
	6	.317	.373	.338	.356	.373	.290
	8	.323	.319	.340	.357	.339	.254
	10	.325	.325	.317	.330	.317	.240
−6.5	1	.377	.382	.412	.341	.363	.346
	2	.322	.328	.273	.261	.261	.272
	3	.258	.259	.246	.216	.234	.261
	4	.249	.260	.249	.215	.202	.215
	5	.230	.230	.180	.188	.208	.227
	6	.222	.222	.228	.186	.197	.194
	8	.225	.225	.198	.164	.168	.164
	10	.216	.200	.195	.154	.154	.154

*All values in this table are of −V; thus all values of V are negative, i.e., directed downward.

TABLE A-6

Pressure probe Measurements of W(m/s) for Pattern No. 6 (Table 1)

x/H

x/H	y/H	2	4	6	10	16	28
0	1	0	.068	.072	.155	.168	.178
	2	0	.082	0	.083	.175	.184
	3	0	0	0	.093	.094	.189
	4	0	0	0	.101	.100	.100
	5	.107	0	.105	.105	.105	.104
	6	.108	0	.108	.107	0	.107
	6	0	0	.111	.111	.109	.111
	10	0	0	.114	.113	.113	.113
-2.5	1	.742	.741	.429	.348	.265	0
	2	.369	.364	.182	.277	.187	0
	3	.100	.098	.194	.194	.097	.097
	4	.103	.102	.101	.101	.101	.100
	5	.105	.104	.105	.104	.104	.104
	6	.106	.106	.105	.105	0	.106
	8	.109	.109	.107	.108	0	.109
	10	.224	.112	.112	.112	0	.112
-4.5	1	.745	.647	.632	.659	.568	.184
	2	.607	.603	.506	.610	.610	.501
	3	.418	.517	.519	.524	.527	.208
	4	.426	.426	.426	.535	.535	.211
	5	.524	.434	.434	.434	.437	.216
	6	.332	.331	.331	.331	.441	.220
	8	.225	.225	.337	.337	.449	. .2
	10	.229	.229	.346	.347	.346	.114
-6.5	1	.290	.289	.283	.094	0	0
	2	.309	.307	.205	.101	.101	.100
	3	.212	.211	.212	.105	.105	.104
	4	.217	.214	.217	.108	.108	.108
	5	.222	.222	.110	0	0	0
	6	.224	.224	.111	0	0	0
	8	.114	.114	.113	0	0	0
	10	.115	.115	.115	0	0	0

Wake Characteristics

Pattern No.		x/H					
		2	4	6	10	16	28
1	δ_1/H	2.2	2.7	3.1	3.6	4.4	5.6
	δ_s/H	1.2	1.1	1.4	1.5	1.7	2.7
	A	.95	.69	.55	.45	.32	.23
	δ_m/H	1.5	1.5	1.9	2.1	2.4	2.7
	$u'_m/U°$	5.2	4.8	4.5	3.9	3.5	2.5
2	δ_1/H	3	3	3.2	4	4	4.8
	δ_s/H	.8	.95	1.2	1.5	1.7	2.6
	A	.5	.49	.43	.32	.29	.21
	δ_m/H	1.5	1.5	1.9	1.9	1.9	2.6
	$u'_m/U°$	4.3	4.1	4.0	3.6	3.2	2.4
3	δ_1/H	2	2.5	2.6	3.2	3.5	4.2
	δ_s/H	1	1.1	1.2	1.4	1.7	2.1
	A	.87	.65	.45	.29	.25	.14
	δ_m/H	1.2	1.5	1.5	1.5	1.9	2.4
	$u'_m/U°$	4.7	4.3	3.8	3.1	2.8	2.2
4	δ_1/H	2	2.4	2.6	2.9	3	3.5
	δ_s/H	.6	.7	.9	1.05	1.1	1.1
	A	.72	.39	.31	.23	.22	.14
	δ_m/H	1.0	1.2	1.2	1.2	1.2	1.2
	$u'_m/U°$	3.9	3.5	3.2	2.8	2.6	2.3
5	δ_1/H	2.9	3.4	3.5	3.8	3.9	4.8
	δ_s/H	.95	.95	1.1	1.3	1.8	2.5
	A	.51	.43	.39	.31	.27	.18
	δ_m/H	1.5	1.5	1.5	1.9	1.9	2.4
	$u'_m/U°$	4.4	4.2	3.9	3.5	3.1	2.5
6	δ_1/H	3.8	4.3	4.7	4.7	5.1	5.8
	$\delta_s/$	.85	1.1	1.5	1.8	2.2	2.9
	A	.43	.40	.39	.35	.31	.22
	δ_m/H	1.9	1.9	2.4	2.4	2.4	3.3
	$u'_m/U°$	4.5	4.4	4.1	3.6	3.3	2.5
7	δ_1/H	4.9	4.8	4.9	5.1	5.2	5.5
	δ_s/H	.75	.96	1.3	1.7	2	2.7
	A	.41	.38	.38	.35	.33	.24
	δ_m/H	1.2	1.5	1.9	2.4	2.4	3.3
	$u'_m/U°$	4.4	4.3	4.1	3.7	3.4	2.5
8	δ_1/H	2.3	2.7	3	3.8	4.6	5.9
	δ_s/H	1.1	1.1	1.25	1.6	1.8	2.8
	A	.89	.72	.50	.51	.42	.29
	δ_m/H	1.5	1.5	1.9	1.9	2.4	3.3
	$u'_m/U°$	4.8	4.9	4.9	4.3	4.0	3.0

TABLE A-7 (Concluded)

Pattern No.		x/H					
		2	4	6	10	16	28
9	δ_1/H	2.5	2.5	2.7	2.7	2.9	4
	δ_s/H	.55	.5	.5	.55	.8	1.1
	A	.14	.16	.17	.19	.20	.17
	δ_m/H	.1	.2	.5	1.0	1.2	1.9
	u'_m/U^*	2.5	2.6	2.6	2.7	2.7	2.6
10	δ_1/H	2.5	2.5	2.9	3.3	3.3	3.6
	δ_s/H	.5	.55	.55	.8	.95	1.3
	A	.16	.19	.19	.20	.21	.18
	δ_m/H	.8	.8	.8	1.2	1.2	1.9
	u'_m/U^*	2.5	2.6	2.7	2.8	2.8	2.5
11	δ_1/H	2.3	2.8	2.7	3	3.3	3.8
	δ_s/H	.75	.75	.85	.95	1	1.5
	A	.19	.20	.25	.24	.22	.20
	δ_m/H	.9	.9	1.2	1.5	1.5	1.9
	u'_m/U^*	2.5	2.6	2.6	2.8	2.8	2.6
12	δ_1/H	2.2	2.8	3.5	4.4	4.9	6
	δ_s/H	1.1	1.2	1.3	1.7	2.3	3
	A	1	.77	.58	.47	.42	.27
	δ_m/H	1.5	1.9	1.9	2.4	2.4	3.3
	u'_m/U^*	5.4	5.0	5.0	4.4	3.9	2.9
13	δ_1/H	2.3	2.8	3.2	3.9	5	5.7
	δ_s/H	1.2	1.25	1.3	1.7	2	2.8
	A	1.2	.93	.59	.5	.38	.26
	δ_m/H	1.5	1.5	1.9	1.9	2.4	3.3
	u'_m/U^*	5.3	4.9	4.8	4.1	3.8	2.8